

Interconnected Air Suspensions with Independent Height and Stiffness Tuning

By

Peyman Karimi Eskandary

A thesis
presented to the University of Waterloo
in fulfillment of the
thesis requirement for the degree of
Master of Science
in
Mechanical Engineering

Waterloo, Ontario, Canada, 2014

© Peyman Karimi Eskandary 2014

AUTHOR'S DECLARATION

I hereby declare that I am the sole author of this thesis. This is a true copy of the thesis, including any required final revisions, as accepted by my examiners.

I understand that my thesis may be made electronically available to the public.

Peyman Karimi Eskandary

Abstract

Suspensions play a crucial role in vehicle comfort and stability. Different types of suspensions have been proposed to fulfill the essential characteristics of vehicle suspensions. A semi-active suspension with adjustable damper improves the performance of a suspension in different conditions and it is better than a passive suspension in terms of ride comfort and handling. Furthermore, it is not as expensive and complicated as an active suspension. Semi-active suspensions rely on adjustable damping coefficient. A new type of air suspension with independent ride height and stiffness tuning has been developed recently. By using two air chambers in the suspension system, ride height of vehicle and stiffness of suspension can be adjusted independently and simultaneously. The conventional air suspension systems use compressor to pump the air into a single flexible rubber airbag and by inflating the air, the chassis will be raised from the axle (ride height control). In this type of suspensions, the stiffness of spring is not under control. In the new air suspension system, by controlling the air pressure on both chambers, one can tune the suspension stiffness and the ride height of the vehicle at the same time for different driving conditions. The air suspension is also able to maintain the vehicle body at the same height and natural frequency for different load or number of passengers. This thesis discusses about the design analysis of an air suspension with ride height and stiffness tuning. The analytical formulation is developed for the optimum design of the new air suspension system.

In this thesis, the interconnection between the pressurized chambers of the new air suspension with ride height and stiffness tuning is studied to further improve the performance. Proper interconnection of air springs can help the suspension system to distribute the load between tires more evenly on rough roads or uneven surfaces. Different configurations in air spring interconnection have different impact on the handling and tire load distribution. To study the effect of air spring interconnection configurations on tires load

distribution and vehicle handling, a general mathematical model is developed. This model is used to compare various configurations in detail.

Results show that interconnection could improve tire load distributions greatly. It is also shown that improving tire load distribution will deteriorate roll stiffness that in turn deteriorate vehicle handling at higher speeds. Since on rough roads, vehicle's speed is necessarily low, interconnection will not have adverse effects on vehicle handling when activated.

Acknowledgements

I would like to thank my supervisor, Professor Amir Khajepour, for great advice, support, and patience that he has shown during my studies. Truly, I would not have been able to finish this thesis without his help.

I would also like to thank my friends and colleagues. In particular, I would like to extend my gratitude to Adrian Wong, Saeid Khosravani, and Alireza Kasaiezadeh for their remarkable help towards finishing this thesis.

Lastly and most importantly, to my parents and brothers, thank you for supporting me from far away. I really appreciate your kindness during my studies. And also, to the best friend that I have ever had, Ashkan Hajjam, thank you for everything you have done for me all these years. Words cannot express my appreciation for my family and friends.

Table of Contents

AUTHOR'S DECLARATION	ii
Abstract	iii
Acknowledgements	v
Table of Contents	vi
List of Figures	ix
List of Tables.....	xi
Chapter 1 Introduction	1
Chapter 2 Literature Review	4
2.1 Ride comfort	4
2.2 Handling	4
2.3 Suspension Systems.....	5
2.3.1 Passive Suspension.....	5
2.3.2 Semi-active Suspension.....	6
2.3.3 Active Suspension.....	6
2.4 Suspension Design Based on Half Car Model Formulation.....	6
2.4.1 Guidelines.....	7
2.4.2 Independent suspension Design	8
2.4.3 Damping Coefficient Design.....	10
2.5 Air Suspension.....	10
2.6 Interconnected Suspension System	12
Chapter 3 Modeling and Design of Air Suspensions with Independent Ride Height and Stiffness Tuning	14

3.1	Basic Formulation.....	14
3.2	Design Criteria.....	16
3.2.1	Minimum Equilibrium Pressure	17
3.2.2	Minimum Natural Frequency	19
3.2.3	Maximum Natural Frequency	20
3.3	Minimum Accumulator Volume	22
3.4	Determining the Cylinder Area and Damper Area.....	23
3.5	Behavior of Air suspension During Extension and Compression	24
3.6	Extra Load	26
3.7	Ride Height Tuning	28
3.8	Numerical Solutions	29
Chapter 4	Effect of Interconnected Air Suspensions on Vehicle Performance	31
4.1	System Modeling with an Independent Air Suspensions	31
4.2	Interconnected Air Chambers.....	37
4.2.1	Load Distribution	42
4.3	Main Interconnection Configurations Comparison	43
4.3.1	Modal Analysis	46
4.3.2	Road Simulations	47
4.4	Interconnection Configurations Comparison.....	50
4.5	Lower Order Model Analysis	51
4.5.1	Truck Pitch Model.....	55

4.5.2	Truck Roll Model	62
Chapter 5	Conclusion and Future Work	67
	Bibliography.....	68
	Appendix 1	72
	Appendix 2	73

List of Figures

Figure 1- Air suspension system with two air chambers	2
Figure 2- Overall Schematic of air-spring for sedan vehicle	3
Figure 3- Half car model with two degrees of freedom.....	7
Figure 4- Decoupled half car model for front and rear suspensions.....	9
Figure 5- Suspension with air spring and auxiliary volumes [21]	11
Figure 6- Schematic of air suspension with dual chamber	14
Figure 7- V_1 - V_2 curve, the accumulators' volume	19
Figure 8- V_1 - V_2 curve and region for minimum pressure and natural frequency.....	20
Figure 9- V_1 - V_2 curve and region for minimum and maximum natural frequency.....	21
Figure 10- Accumulators' volume versus damper area.....	24
Figure 11- possible solutions for accumulators' volume	30
Figure 12- Truck model with three axles	31
Figure 13- different types of pneumatic spring.....	32
Figure 14- Independent air chambers	37
Figure 15- Connected air chambers	37
Figure 16- Top view of truck and interconnection indexes	38
Figure 17- Second right rear tire force ratio respect to first right rear tire	44
Figure 18- First left rear tire force ratio respect to first right rear tire	45
Figure 19- Second left rear tire force ratio respect to first right rear tire.....	45
Figure 20- Different types of the roads.....	48
Figure 21- Quarter car model with unsprung mass.....	52
Figure 22- Quarter car model without unsprung mass.....	53
Figure 23- Bode plot of quarter car models	54
Figure 24- Half car model for three axle truck	55
Figure 25- Rear tires force ratio.....	60
Figure 26- Pitch motion of sprung body.....	62

Figure 27- Front view of truck.....	62
Figure 28- Right and left tires force ratio	65
Figure 29- Roll angle of sprung body	66
Figure 30- Dual chamber air suspension schematic	72

List of Tables

Table 1- Typical passenger car specification.....	18
Table 2- Main interconnection configurations.....	42
Table 3- Heavy truck specification.....	43
Table 4- System natural frequencies based on the eigenvalues of system	46
Table 5- Road classification.....	47
Table 6- RMS rear tire force with different main interconnection configurations	48
Table 7- Maximum rear tires force with different main interconnection configurations	49
Table 8- Bounce, pitch, and roll motion of body	49
Table 9- Different configurations for roll interconnection	50
Table 10- Different configurations for pitch interconnection.....	50
Table 11- Different configurations for cross and all interconnection.....	51
Table 12- Heavy truck specification for pitch model	59
Table 13- Heavy truck specification for roll model.....	64

Chapter 1 Introduction

The main purpose of any suspension system is isolation of the vehicle's body from the vibration induced from road unevenness. There are many standards to define appropriate measurable criteria for the performance of suspension systems. It is clear that very stiff suspension and high damping are suitable for better vehicle handling and stability, while very soft spring and low damping are more appropriate for ride comfort. Therefore, the design of a suspension is a compromise between vehicle's comfort and handling. Semi-active suspension systems by using adjustable dampers provide better comfort and handling depending on road conditions. It should be mentioned that active suspension systems could eliminate a compromised design of suspensions by actively providing the desired force between the wheel and chassis. These suspensions however are more expensive and complicated.

This thesis is a study on design analysis of an air suspension with ride height and stiffness tuning. As this system should be able to tune two parameters (ride height and stiffness) independently, it needs two air chambers (pneumatic spring). By using two air chambers and controlling the air pressure independently in each chamber, suspension stiffness and ride height of the vehicle can be adjusted independently and simultaneously for different driving conditions. There are various geometrical configurations for two air chambers around axle.

Figure 1 shows general configuration of air suspension system with ride height and stiffness tuning containing two air chambers. This suspension system works based on the motion of a four-bar mechanism with extended trailing arm (the blue lever). Increasing the air pressure in both chambers makes the system stiffer. Also, discharging and charging the left and right chambers respectively, turns the lever clockwise. As a result, the ride height will be increased. It is obvious that the force from air chambers should satisfy the force equilibrium equation for trailing arm, at any time. Therefore the pressures should be set accurately to obtain the desired ride height and suspension stiffness.

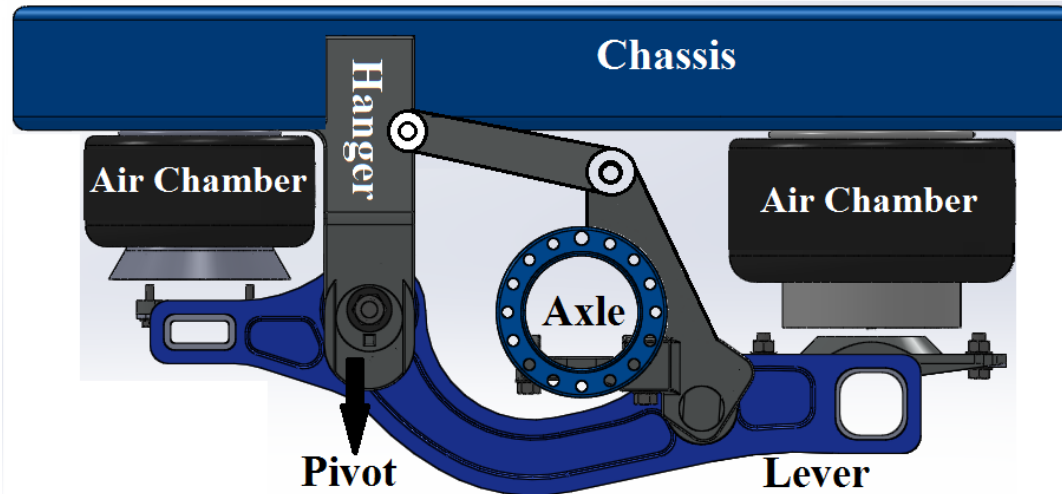


Figure 1- Air suspension system with two air chambers

However, some constraints and conditions make the procedure of design difficult; the height of the center of gravity, ground clearance, the space for suspension in the vehicle body, and suspension travel are some of these parameters. In some cases, it is required to change the suspension mechanism and the air chambers locations. For instance, heavy trucks have enough space around their axle and at the bottom of chassis. Therefore, air springs are placed on both sides of the axle, as shown in Figure 1. But, in passenger vehicles the geometrical constraints are critical and the air suspension system including the air chambers should be compact; therefore, it is preferred to combine the chambers in a single cylinder. This cylinder is divided to two chambers by a piston. The pressure of each chamber will be adjusted by a pressure regulator valve. As Figure 2 shows, the compressor supplies high pressure air which is stored in the main tank. Then the regulator valves use the compressed air to adjust the pressure of air chambers. Moreover, the accumulators that are connected to the chambers help the air suspension system cover a wide range of desired stiffness.

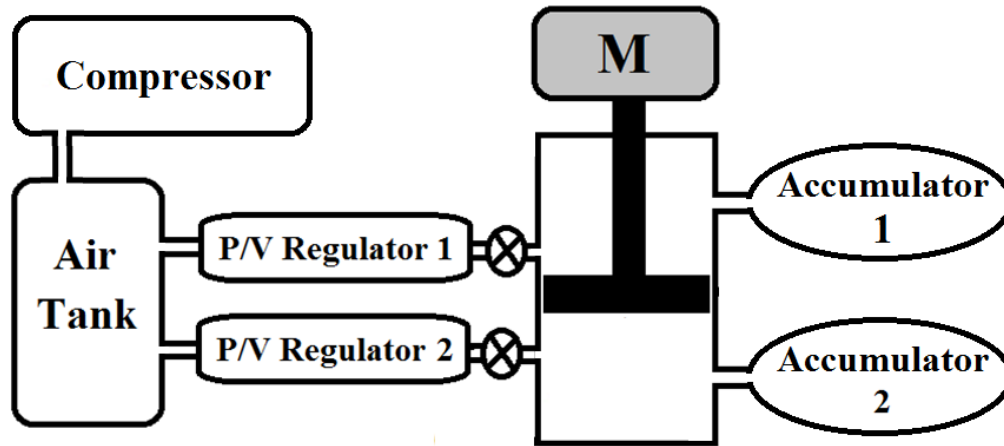


Figure 2- Overall Schematic of air-spring for sedan vehicle

The interconnection between the pressurized air chambers is another advantage of air suspension system. Interconnection results in equalization of pressure in the chambers. The pressure of interconnected air chambers will be the same all the time since the air pressure loss in connections and fittings is negligible, which is conventional assumption for a pneumatic system. The proper interconnection of air springs can help the suspension system to distribute the load more evenly between tires on poor condition roads. Splitting the load between the tires has a crucial role in increasing the safety of suspension system and reducing the weight of suspension components. Different configurations in air spring interconnection have different impact on the handling and tire load distribution. The analysis of different interconnection configurations in air suspensions with ride height and stiffness tuning will also be studied in this thesis. The general mathematical model developed for a heavy truck with three axles is used to do this analysis. The model can be simplified or extended for other vehicles.

Chapter 2 is a review of the literature and discusses the related work in this field. Chapter 3 presents modeling and design of air suspension systems with independent ride height and stiffness tuning. Based on the mathematical model, the accumulators' volume and air chambers pressure will be calculated. Chapter 4 demonstrates the model for heavy trucks with three axles that takes the advantage of interconnection between the air suspension systems with independent ride height and stiffness tuning. This chapter studies the impact of different interconnection configurations on the vehicle handling and suspension performance. Lastly, Chapter 5 is conclusion and a brief discussion of future work.

Chapter 2 Literature Review

Suspension system has a significant influence on passengers' comfort and vehicle performance. Generally, suspension system consists of three essential elements: spring, damper, and linkages. Each one has crucial role in suspension performance. Spring makes system softer and stores the energy. Damper settles system down and dissipates the energy. The linkages constraint system motion based on the required geometrical limits and characteristics for vehicle. The main characteristics of a suspension system are ride comfort and handling.

2.1 Ride comfort

There are four methods to evaluate ride comfort (also referred to as human response to vibration [1]). A commonly used method is the ISO 2631 standard [2], although there are other standards such as BS 6841[3], VDI 2057 [4] and AAP [5]. It seems that the most important measurable parameter for the ride comfort is vertical displacement and acceleration. The acceleration of vehicle body versus frequency and RMS of acceleration are appropriate characteristics to judge the ride comfort of a vehicle. In other word, ride comfort is proportional to the absolute acceleration of vehicle body. Likewise, settling time of vehicle body is important in ride comfort [6]. For heavy trucks, ride comfort is defined by pitch plane motion versus lateral and roll vibration [7].

2.2 Handling

Handling is defined as the percentage of the available friction of tires or the maximum achievable lateral acceleration. At values lower than the linearity limit, the vehicle behaves in linear mode. However, at values higher than the friction limit of tires, control over the vehicle is physically impossible and even the most experienced driver in the well-handling vehicle will lose control. The responsibility of the vehicle designer is to achieve two aims: to raise the absolute friction limit of tires, and to increase the linearity limit [1].

Handling tests is divided into two main categories: steady state handling tests and dynamic handling tests (also called transient response tests). The steady state handling test is the constant radius test, where the vehicle is driven around a circle. The most important parameters that need to be measured are steering wheel angle and lateral acceleration. The test starts at a low speed.

Speed is gradually increased until the vehicle cannot move in a constant radius. A graph of lateral acceleration against vehicle speed is used to show whether the vehicle is over-steering, under-steering, or showing neutral behavior. Dynamic handling tests can be either closed-loop (where a driver tries to steer the vehicle through a prescribed path), or open loop (where steering angle vs. time is determined). Closed loop tests include the double lane change test and obstacle avoidance test. Open loop tests can be done by an experienced driver or a robot. These include the step steer and pulse steer tests [1]. One of the most important measurable parameters for handling is the normal force of tires; minimum values play an important role in the judgment of vehicle handling.

2.3 Suspension Systems

There is an extensive literature on suspension systems. The following section has a quick look over different suspension systems that generally can be categorized into three different types: passive, semi-active, and active. Each one has its own benefits and drawbacks.

2.3.1 Passive Suspension

A passive suspension, or conventional suspension, is an isolator unit between the tire and vehicle body to absorb and minimize the vibration by using a spring (e.g., a coil spring) and a damper. A common element of all passive systems is that the control of suspension is not possible, and that the system cannot be tuned for better performance while operating. A passive suspension is simple in term of design, and more cost effective in manufacturing and maintenance costs; this is why most companies use passive suspension systems [8]. It also does not consume energy or have a controller.

Plenty of research has been conducted on the compromising ride comfort and handling of vehicles with passive suspension system. For example, Gobbi [9] applied numerical optimization to find the best values for a conventional passive suspension by using a quarter car model. It was concluded that the semi-active elements [10] like variable damper [11] can improve the design more than the passive suspension.

2.3.2 Semi-active Suspension

Semi-active suspension systems have adjustable elements like damper, which can be tuned to improve the performance of the suspension in different road conditions. For instance, in off-road condition, damping coefficient can be decreased to improve ride comfort. Likewise, in flat roads, handling can be improved using a stiff damper. There are several options to have a variable damping coefficient. Firstly, the Magneto Rheological damper (MR damper) has iron particles in oil, and changing the magnetic field in the dash pot can regulate the flow rate of oil through the dash pot, as well as the damping coefficient [12, 13]. The second option is utilizing the damper with a variable area orifice [14]. Ultimately, it should be mentioned that semi-active suspensions do not have a force actuator; therefore, they cannot enforce the system to behave as desired.

2.3.3 Active Suspension

An active suspension has a hydraulic, electro-mechanic, pneumatic, or electric actuator in addition to or instead of spring and damper. However, most vehicle companies prefer to use the hydraulic system as the force actuator. The role of this actuator is to apply controlled force to the sprung mass; it is generally placed at the same location as the spring and damper are, between the unsprung mass (hub) and sprung mass (body). There are several methods to control the actuator to optimize the operation of suspension and minimize the vibration of the body. While most luxury cars have an active suspension, the power consumption of active suspension needs to be considered.

2.4 Suspension Design Based on Half Car Model Formulation

In order to design a suspension and determine the best values for each element, the spring stiffness is first evaluated. Then, by using the spring rate, the damping coefficient is calculated. Consider the vehicle shown in Figure 3, for simplicity in the equations, the tire mass is assumed negligible.

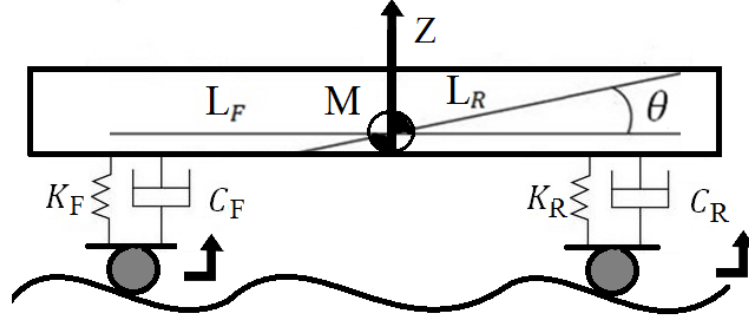


Figure 3- Half car model with two degrees of freedom

Based on the Newton-Euler equations about center of mass, the differential equations for the bounce (Z) and pitch (θ) motions can be written as:

$$\begin{aligned}
 \ddot{Z} + \alpha Z + \beta \theta &= 0 \\
 \ddot{\theta} + \frac{\beta Z}{k^2} + \gamma \theta &= 0
 \end{aligned} \tag{2.1}$$

$$\alpha = \frac{K_F + K_R}{M} \quad \beta = \frac{K_R L_R - K_F L_F}{M} \quad \gamma = \frac{K_F L_F^2 + K_R L_R^2}{M k^2} \quad k = \sqrt{\frac{I_y}{M}}$$

I_y is pitch moment of inertia about the lateral axis of the vehicle, and k is the gyration radius of the vehicle. Moreover, M is the mass of the half vehicle.

By solving the Newton-Euler equations:

$$\begin{aligned}
 \omega_{Bounce} &= \sqrt{\frac{\alpha + \gamma}{2} + \sqrt{\frac{(\alpha - \gamma)^2}{4} + \frac{\beta^2}{k^2}}} \\
 \omega_{Pitch} &= \sqrt{\frac{\alpha + \gamma}{2} - \sqrt{\frac{(\alpha - \gamma)^2}{4} + \frac{\beta^2}{k^2}}}
 \end{aligned} \tag{2.2}$$

It is easy to distinguish between bounce frequency and pitch frequency based on the location of oscillation centers [7].

2.4.1 Guidelines

Based on Maurice Olley's instructions [15], there are some useful guidelines for the design procedure of suspensions:

- 1- The front spring should be 30% less stiff than the rear spring, or the spring center should be at least 6.5% of the wheelbase, behind the center of mass.
- 2- The pitch and bounce frequencies should be close together, and the bounce frequency should be less than 1.2x the pitch frequency.
- 3- Both frequencies should not be greater than 1.3 Hz, and also the static deflection of the suspension should not exceed 15 cm.

The natural frequency of the front and rear suspension is defined:

$$\omega_F = \sqrt{\frac{K_F}{M_F}} \quad \omega_R = \sqrt{\frac{K_R}{M_R}} \quad (2.3)$$

$$M_F = M \frac{L_R}{L_R + L_F} \quad M_R = M \frac{L_F}{L_R + L_F}$$

where L_F and L_R are the front and rear wheels distance from center of mass, respectively..

In most sedan vehicles, the weight distribution between the front and rear wheels leads to:

$$M_F = 0.55M \rightarrow L_F = 0.45L \quad M_R = 0.45M \rightarrow L_R = 0.55L \quad (2.4)$$

where L is the wheelbase of the vehicle.

Furthermore, other instructions for suspension design state that the best ratio of rear frequency to front frequency is 1.2 [16].

$$\frac{\omega_F^2}{\omega_R^2} = \frac{\frac{K_F}{M_F}}{\frac{K_R}{M_R}} = \frac{K_F M_R}{K_R M_F} = \left(\frac{1}{1.2}\right)^2 \Rightarrow \frac{K_F}{K_R} = \frac{1 \times 0.55}{1.44 \times 0.45} = 0.85 \quad (2.5)$$

It seems that the best ratio for the front spring stiffness to the rear one is 0.85, which satisfies all of the instructions and requirements.

2.4.2 Independent suspension Design

The most important issue in the evaluation of bounce and pitch frequencies is the value of the moment of inertia. The half car model could be represented as a discrete mass model.

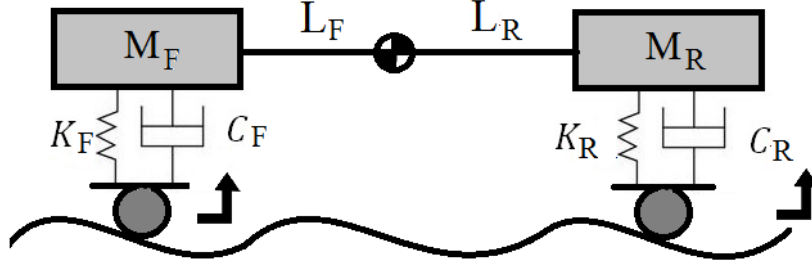


Figure 4- Decoupled half car model for front and rear suspensions

Considering Figure 4, the moment of inertia about CG for a discrete mass model is:

$$I_{y-discrete} = M_F L_F^2 + M_R L_R^2 = M \frac{L_R L_F^2}{L_R + L_F} + M \frac{L_F L_R^2}{L_R + L_F} = M L_R L_F \quad (2.6)$$

Therefore, the radius of gyration is:

$$k(\text{gyration radius}) = \sqrt{\frac{I_y}{M}} = \sqrt{L_R L_F} \quad (2.7)$$

For instance, values of parameters for a passenger sedan vehicle are [17]:

$$\begin{aligned} M &= 1460 \text{ (Kg)} & L_F &= 1.3 \text{ (m)} & L_R &= 1.4 \text{ (m)} \\ I_{yy} &= 2460 \text{ (Kg.m}^2\text{)} & M L_R L_F &= 2657 \text{ (Kg.m}^2\text{)} \end{aligned} \quad (2.8)$$

Thus, it can be said:

$$I_y \simeq M L_R L_F \quad (2.9)$$

By considering this fact, the front and rear suspensions can be designed independently and the bounce and pitch frequencies are equal with the rear and front suspension frequencies:

$$\begin{aligned} \omega_F = \omega_{Pitch} &= \sqrt{\frac{K_F (L_R + L_F)}{L_R M}} \\ \omega_R = \omega_{Bounce} &= \sqrt{\frac{K_R (L_R + L_F)}{L_F M}} \end{aligned} \quad (2.10)$$

2.4.3 Damping Coefficient Design

In order to determine the damping coefficient of a damper, usually the damping ratio for passenger cars is considered between 0.2 up to 0.4. With this range of damping ratio, the ratio of damped natural frequency to undamped natural frequency is between 0.92 and 0.98 [16].

$$\zeta_F = \frac{C_F}{\sqrt{4K_F M_F}} \quad \zeta_R = \frac{C_R}{\sqrt{4K_R M_R}} \quad (2.11)$$

2.5 Air Suspension

Pneumatic spring or air spring is a device that uses the compressibility of gas as a spring. Due to the fast motion of suspension, the compression and expansion is rapid and there is not enough time for heat transfer; therefore, it can be assumed that the gas process is isentropic:

$$\begin{aligned} PV^\gamma &= \text{constant} \\ \gamma &= 1.4 \end{aligned} \quad (2.12)$$

At first, by adjusting the amount and pressure of gas in the air spring, the system will be leveled at the desired height. Normal static pressure is about 3 bars, and will not reach more than 7- 8 bar (100- 120 psi) [19].

The exerted force by the airbag is the effective area of airbag multiplied by the air pressure. However, the effective area of airbag is not constant over its compression and extension, and it is not a linear function of air pressure [20]. Generally, it can be said that by increasing the air pressure, the effective area would be increased.

Hrishikesh V Deo [21] conducted research on semi-active suspensions with an air spring.

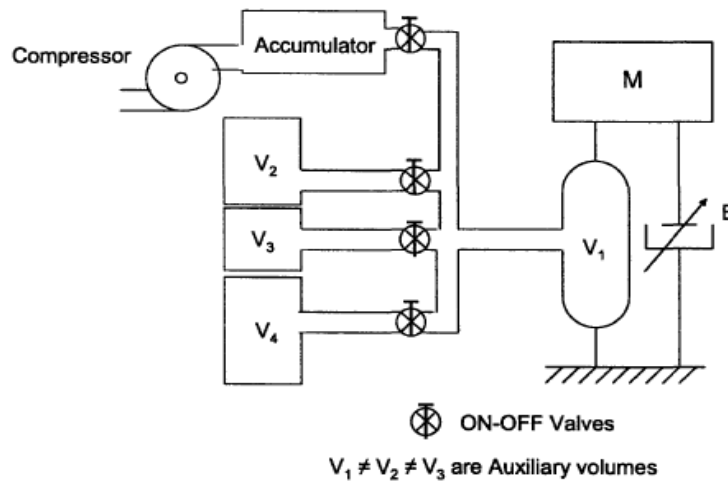


Figure 5- Suspension with air spring and auxiliary volumes [21]

As Figure 5 demonstrates, by connecting each or some of the extra volumes to the main spring, the stiffness of suspension can be adjusted.

Toyofuku and Yamada [22] proposed an analytical model for air suspension with auxiliary volumes, considering the effect of pipes and connections. Their research showed that the auxiliary chamber has a smaller effect on the system in high frequencies than low frequencies.

Giliomee [23] developed a semi-active hydro pneumatic spring and damper system for off-road vehicles by using hydro pneumatic spring and hydraulic damper. The system works based on two solenoid valves on damper and spring, which can adjust the damping coefficient and spring stiffness. This system also has two accumulators for high pressure air. These accumulators can make some problems in terms of space and packing.

Ramsbottom [24] proposed a pneumatic suspension, electronically controlled, that comprises a variable spring rate system, switchable damping and load leveling. Results show performance improvement for roll behavior of vehicle.

Porumamilla [25] presented a novel concept for air suspension system. They have used an air-spring-orifice-accumulator to change the stiffness and also damping coefficient. Therefore, in this system, damper is not needed. This system named Continuously Variable Natural Frequency and Damping (CVNFD). The simulation results and experiments show this system is able to

change suspension stiffness continuously and independently. They believe this system has a better performance even than MR damper.

Yin and his colleagues [26] developed a comprehensive model for air suspension with accumulator and orifice valve. At the first step, they modeled the system based on the solid cylinder divided to two separated chambers by a piston and the pressure in each chamber can be regulated by a pressure regulator valve. Each side of piston is connected to an accumulator as well. At this step the orifice valve has not been considered. In the next step, Yin studied the damping behavior of system when the pressurized gas passes through the orifice valves which are on each side of piston.

Then they applied their model on the practical design. The experimental results present good achievements on the conceptual and detail design. In their experiment procedure, they try to identify the system parameters based on the experimental data and tune the model.

2.6 Interconnected Suspension System

Hawley [27] in 1927 proposed the interconnection of air springs in the roll and pitch plane, which is also called roll and pitch interconnection, respectively. He also introduced the cross interconnection. In 1949, Citroen Co. started to use pitch interconnection [28] in their vehicles, and later, several studies were conducted on the interconnection concept. Following this, Toyota and Nissan used active suspension with pneumatic and hydraulic interconnection in the 1980s [29, 30].

In 1992, Bhave [31] completed parametric modeling to study the effects of pitch interconnection on ride comfort and vehicle performance. In 1997, Ortize [32] discussed about many configurations of interconnection for sedan vehicle by using hydraulic equipment and mechanical linkages. He proposed the conceptual design but he did not do the modeling and experimental research.

Recently, Cao and his colleagues have been conducted at Concordia University on pitch and cross interconnection for heavy vehicles [33-36]. The researchers modeled details of system such as pressure losses in hydraulic lines and valves. They used the polytrophic process to describe the thermodynamic behavior of gas in a system, and also completed simulations for different

road profiles in time domains to determine the advantages of interconnection compared to conventional suspension systems.

Cao has studied the roll- and pitch-plane-coupled hydro pneumatic suspension and they have considered too many different configurations for interconnection of pneumatic suspension systems. By comparing them from various aspects, good decision can be made based on the application of vehicle.

HIS or Hydraulically Interconnected Suspension systems is a popular concept in articles related to interconnection. Ding and colleagues [37] presented the HIS model to reduce the roll motion of heavy trucks with three axles (tri-axle). They considered all details in their parametric models and studied the modal analyses of both HIS and conventional systems.

Chapter 3 Modeling and Design of Air Suspensions with Independent Ride Height and Stiffness Tuning

The goal of this chapter is to design an air suspension with ride height and stiffness tuning. As discussed in introduction, there are various geometrical configurations for two air chambers around axle. In this chapter, the modeling and formulation is based on the combined chambers in a single cylinder. This cylinder is divided to two chambers by a piston.

3.1 Basic Formulation

Figure 6 illustrates the schematic of the air spring with independent ride height and stiffness tuning, which employs a pneumatic cylinder for vertical configuration. This system was first proposed in [26] and consists of a cylinder, two Pressure/Volume regulators (P/V regulator) which control two chambers Pressure/Volume, and an air tank which is supplying the high pressure air for the system. There are also two valves that separate chambers from the tank and regulators, and two accumulators that are connected to the upper and lower chambers of cylinder.

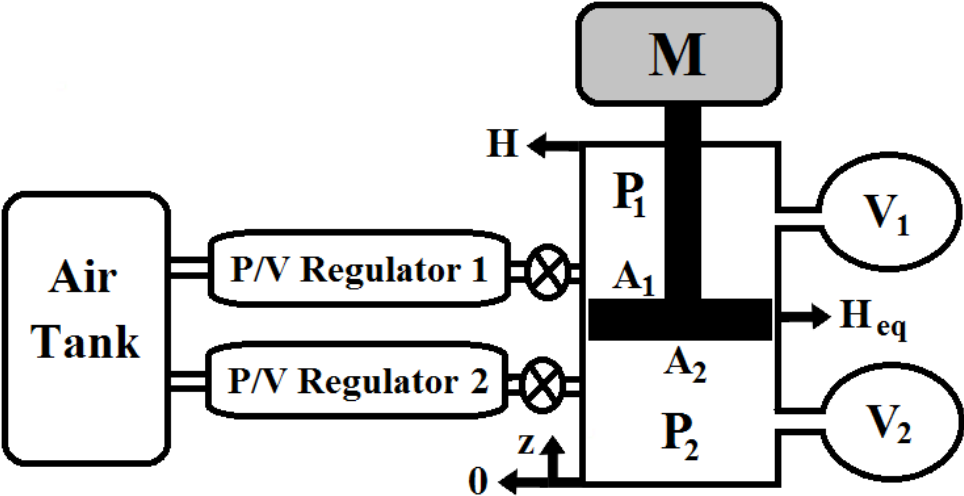


Figure 6- Schematic of air suspension with dual chamber

The force exerted by air spring can be written as:

$$F(z) = (P_2(z) - P_a)A_2 - (P_1(z) - P_a)A_1 \tag{3.1}$$

where $P_2(z)$ and $P_1(z)$ represents the pressures of chamber 2 and chamber 1 respectively, as a function of the piston position (z). A_2 and A_1 are effective areas of corresponding chambers, and P_a is atmospheric pressure.

It is obvious that:

$$A_2 = A_1 + A_{damper} \Rightarrow A_2 > A_1 \quad (3.2)$$

where A_{Damper} is the area of damper which also has the role of rod connected to the piston.

According to the thermodynamic law and considering that the gas mass in each chamber is constant during the extension or retraction, the process of gas can be supposed to be an isentropic process. Therefore, the characteristics of gas are expressed as:

$$PV^\gamma = C \Rightarrow P = \frac{C}{V^\gamma} \quad (3.3)$$

where P is gas absolute pressure, V is the gas volume or volume of each chamber plus the accumulator connected to the chamber, C is a constant value, and γ is the heat capacity ratio of gas. Therefore, this equation can be applied to both chambers:

$$P_1(z) = \frac{C_1}{(V_1 + A_1(H - z))^\gamma} \quad P_2(z) = \frac{C_2}{(V_2 + A_2z)^\gamma} \quad (3.4)$$

where H is the total length of cylinder, z is the piston position measured from the bottom of the cylinder, and C_1, C_2 are constant values.

By substituting the pressure functions in equation (3.1), the exerted force is:

$$F(z) = \left(\frac{C_2}{(V_2 + A_2z)^\gamma} - P_a \right) A_2 - \left(\frac{C_1}{(V_1 + A_1(H - z))^\gamma} - P_a \right) A_1 \quad (3.5)$$

The spring rate or stiffness can be easily derived by calculating the partial derivative of $F(z)$ to the piston position (z):

$$K = -\frac{\partial F}{\partial z} = \frac{C_2\gamma A_2^2}{(V_2 + A_2z)^{\gamma+1}} + \frac{C_1\gamma A_1^2}{(V_1 + A_1(H - z))^{\gamma+1}} = \frac{P_2(z)\gamma A_2^2}{(V_2 + A_2z)} + \frac{P_1(z)\gamma A_1^2}{(V_1 + A_1(H - z))} \quad (3.6)$$

The natural frequency of the suspension is then:

$$f = \frac{\omega_n}{2\pi} = \frac{\sqrt{\frac{K}{m}}}{2\pi} = \frac{\sqrt{\frac{\frac{P_2(z)\gamma A_2^2}{(V_2 + A_2 z)} + \frac{P_1(z)\gamma A_1^2}{(V_1 + A_1(H - z))}}{m}}}{2\pi} \quad (3.7)$$

where m is a part of vehicle sprung mass on each suspension and f is natural frequency of suspension.

The most important part of modeling of the air suspension is evaluation of $P_2(z)$ and $P_1(z)$ by solving the sets of equations for natural frequency and force equilibrium. This results in:

$$\left\{ \begin{array}{l} F_{(at\ z=H_{eq})} = mg \Rightarrow mg = (P_{eq2} - P_a)A_2 - (P_{eq1} - P_a)A_1 \\ f_{(at\ z=H_{eq})} = f_s \Rightarrow f_s = \frac{\sqrt{\frac{\frac{P_{eq2}\gamma A_2^2}{(V_2 + A_2 H_{eq})} + \frac{P_{eq1}\gamma A_1^2}{(V_1 + A_1(H - H_{eq}))}}{m}}}{2\pi} \end{array} \right. \quad (3.8)$$

where P_{eq2} and P_{eq1} are equilibrium pressure of chambers:

$$\begin{aligned} P_{eq1} &= \frac{C_1}{(V_1 + A_1(H - H_{eq}))^\gamma} = \frac{(4f_s^2 \pi^2 m (V_2 + A_2 H_{eq}) - A_2 \gamma (A_{damper} P_a + mg))(V_1 + A_1(H - H_{eq}))}{A_1 \gamma (A_1 V_2 + A_2 V_1 + A_1 A_2 H)} \\ P_{eq2} &= \frac{C_2}{(V_2 + A_2 H_{eq})^\gamma} = \frac{(4f_s^2 \pi^2 m (V_1 + A_1(H - H_{eq})) + A_1 \gamma (A_{damper} P_a + mg))(V_2 + A_2 H_{eq})}{A_2 \gamma (A_1 V_2 + A_2 V_1 + A_1 A_2 H)} \end{aligned} \quad (3.9)$$

By setting the equilibrium pressures, the force and natural frequency equations at the equilibrium position can be satisfied. This means, at the equilibrium position, the weight of a car can be handled by the air pressure difference and area difference between two sides of piston (air chambers), and suspension natural frequency is the desired natural frequency (f_s).

3.2 Design Criteria

There are certain criteria that are as important to meet as force equilibrium and natural frequency, such as tuning the natural frequency rang. In different roads such as on-road and off-road, the

natural frequency of the vehicle needs to be changed, and the chambers equilibrium pressures should be feasible.

The first unknown parameters are the accumulators' volume. By using some design criteria, it is tried to find their optimum values.

3.2.1 Minimum Equilibrium Pressure

Not only the both equilibrium pressures should be a positive number, but they also should be greater than the atmospheric pressure (100,000 pa). All of the pressures are in absolute scale and they are not gage pressures.

$$P_{eq1} \geq P_a = 10^5 \text{ pa} \quad P_{eq2} \geq P_a \quad (3.10)$$

The equilibrium pressure of chamber 1 (upper chamber) is less than the second chamber; therefore, by satisfying the minimum pressure condition for P_{eq1} , it is assured that both equilibrium pressures are more than the atmospheric pressure. The new set of equations that meet the minimum pressure condition is:

$$\begin{cases} F_{(at \ z=H_{eq})} = mg \\ f_{(at \ z=H_{eq})} = f_s \\ P_{eq1} \geq P_a \end{cases} \quad (3.11)$$

And the solution of equation (3.11) is:

$$\begin{cases} P_{eq2} \geq \frac{mg + A_2 P}{A_2} \\ V_2 \geq \frac{A_2 \gamma P_a A_1^2 H_{eq} + A_2 (\gamma mg + \gamma A_2 P_a - 4 f_s^2 \pi^2 m H_{eq}) (V_1 + A_1 (H - H_{eq}))}{4 f_s^2 \pi^2 m (V_1 + A_1 (H - H_{eq})) - \gamma P_a A_1^2} \end{cases} \quad (3.12)$$

The second equation shows a valid region for V_1 and V_2 on the V_1 - V_2 plane. The graph is a hyperbola curve shown in Figure 7. The gray region represents valid choices for accumulators' volume:

$$V_2 \geq \frac{aV_1 + b}{cV_1 + d} \rightarrow \begin{cases} a = A_2(\gamma mg + \gamma A_2 P_a - 4f_s^2 \pi^2 m H_{eq}) \\ b = A_2 \gamma P_a A_1^2 H_{eq} + A_1 A_2 (H - H_{eq})(\gamma mg + \gamma A_2 P_a - 4f_s^2 \pi^2 m H_{eq}) \\ c = 4f_s^2 \pi^2 m \\ d = 4f_s^2 \pi^2 m A_1 (H - H_{eq}) - \gamma P_a A_1^2 \end{cases} \quad (3.13)$$

Table 1 shows a typical passenger car specification for the simulations in this chapter.

Table 1- Typical passenger car specification

Description	Symbol	Value	Unit
Vehicle sprung mass on each suspension	m	550	Kg
Extra load on each suspension	m_l	50	Kg
Cylinder height	H	0.14	m
Piston equilibrium height	H_{eq}	0.08	m
Cylinder area	A_2	90	Cm^2
Damper area	A_{damper}	65	Cm^2
Heat capacity ratio of air	γ	1.4	-
Minimum natural frequency	f_{min}	1.0	Hz
Maximum natural frequency	f_{max}	1.5	Hz
Desired natural frequency	f_s	1.25	Hz

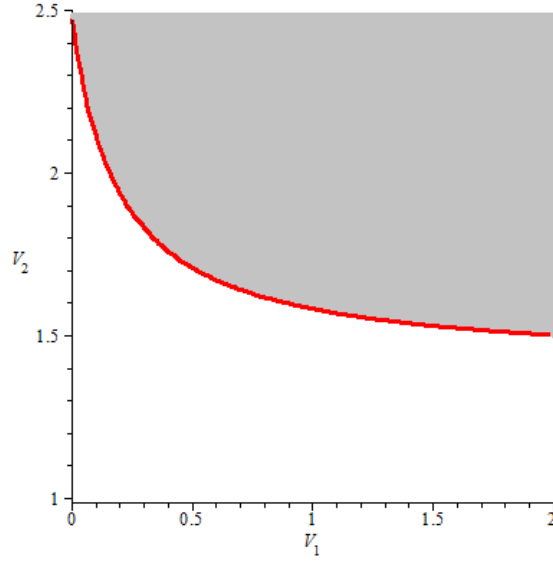


Figure 7- V_1 - V_2 curve, the accumulators' volume

3.2.2 Minimum Natural Frequency

Having a certain minimum natural frequency is necessary to cover the desired range of stiffness range. By decreasing the pressure of both air chambers, the stiffness will be decreased. Therefore, the minimum natural frequency occurs when pressure of the upper chamber (lower pressure) is atmospheric pressure, and the natural frequency is lower bound of desired frequency range. By solving the equations for the minimum natural frequency, the solution for V_1 and V_2 on the $V_1 - V_2$ plane will be:

$$\begin{cases} mg = (P_{eq2min} - P_a)A_2 - (P_{eq1min} - P_a)A_1 \\ P_{eq1min} = P_a \end{cases} \Rightarrow P_{eq2min} = \frac{mg + A_2P}{A_2}$$

$$f_{(at P_{eq1}=P_a)} = f_{\min\text{-desired}} \Rightarrow f_{\min\text{-desired}} = \frac{1}{2\pi} \sqrt{\frac{(P_a A_2 + mg)\gamma A_2 + \frac{P_a \gamma A_1^2}{V_1 + A_1(H - H_{eq})}}{V_2 + A_2 H_{eq}}} \quad (3.14)$$

$$V_2 \geq \frac{aV_1 + b}{cV_1 + d} \rightarrow \begin{cases} a = A_2(\gamma mg + \gamma A_2 P_a - 4f_{\min}^2 \pi^2 m H_{eq}) \\ b = A_2 \gamma P_a A_1^2 H_{eq} + A_1 A_2 (H - H_{eq})(\gamma mg + \gamma A_2 P_a - 4f_{\min}^2 \pi^2 m H_{eq}) \\ c = 4f_{\min}^2 \pi^2 m \\ d = 4f_{\min}^2 \pi^2 m A_1 (H - H_{eq}) - \gamma P_a A_1^2 \end{cases} \quad (3.15)$$

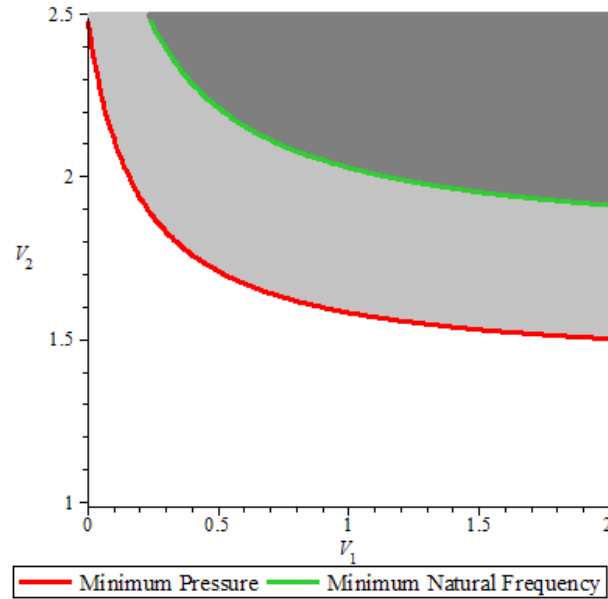


Figure 8- V_1 - V_2 curve and region for minimum pressure and natural frequency

Figure 8 shows the regions that satisfy the conditions talked about. The light gray area can satisfy the minimum pressure, and the dark gray area meets the minimum natural frequency condition while satisfying the minimum pressure condition.

3.2.3 Maximum Natural Frequency

The maximum working pressure of an air spring (the air compressor maximum pressure) is known. Using this maximum pressure in the lower chamber, the maximum natural frequency can be obtained:

$$\begin{cases} mg = (P_{eq2max} - P_a)A_2 - (P_{eq1max} - P_a)A_1 \\ P_{eq2max} = P_{max} \end{cases} \Rightarrow P_{eq1max} = \frac{P_{max}A_2 - P_aA_{damper} - mg}{A_1}$$

$$f_{(at P_{eq2}=P_{max})} = f_{max-desired} \Rightarrow f_{max-desired} = \sqrt{\frac{\frac{P_{max}\gamma A_2^2}{V_2 + A_2 H_{eq}} + \frac{(P_a A_{damper} + mg - P_{max}A_2)\gamma A_1}{V_1 + A_1(H - H_{eq})}}{m}} \quad (3.16)$$

$$f_{(at P_{eq2}=P_{max})} = f_{max-desired} \Rightarrow f_{max-desired} = \frac{m}{2\pi}$$

The solution for V_1 and V_2 on the V_1 - V_2 plane would be:

$$V_2 \leq \frac{aV_1 + b}{cV_1 + d} \rightarrow \begin{cases} a = A_2^2 \gamma P_{max} - 4f_{max}^2 \pi^2 m H_{eq} A_2 \\ b = A_1 A_2^2 \gamma P_{max} H - A_1 A_2 \gamma H_{eq} (mg + A_{damper} P_a) - 4f_{max}^2 \pi^2 m H_{eq} A_1 A_2 (H - H_{eq}) \\ c = 4f_{max}^2 \pi^2 m \\ d = 4f_{max}^2 \pi^2 m A_1 (H - H_{eq}) + A_1 \gamma (mg + A_{damper} P_a - A_2 P_{max}) \end{cases} \quad (3.17)$$

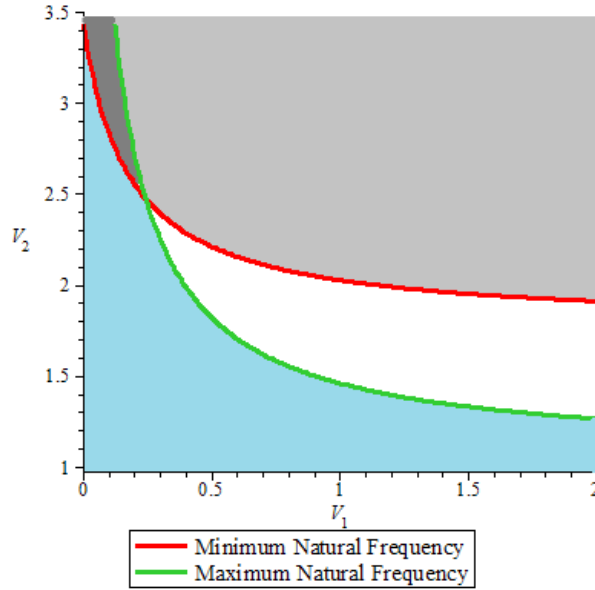


Figure 9- V_1 - V_2 curve and region for minimum and maximum natural frequency

As it is expected, Figure 9 reveals that the blue area under the maximum natural frequency curve is satisfying the maximum natural frequency condition. The dark gray area contains the possible choices for V_1 and V_2 that can satisfy both constraints (maximum and minimum natural frequencies).

3.3 Minimum Accumulator Volume

Figure 9 can be used to find the optimum V_1 and V_2 in the region between the two curves (dark gray area) or on its boundaries (red and green curves above their intersection). The optimum choice of V_1 and V_2 means their minimum value of summation. Therefore, this point on the V_1 - V_2 graph will be on the minimum natural frequency curve because it is the lower boundary of the acceptable region for V_1 and V_2 and it has the least value of summation. To find the minimum accumulators' volume, the derivative of $(V_1 + V_2)$ function based on the minimum natural frequency condition respect to V_1 or V_2 is used:

$$\begin{aligned}
 (V_1 + V_2)_{\min} &\rightarrow \frac{d}{dV_1}(V_1 + V_2) = \frac{d}{dV_1}\left(V_1 + \frac{aV_1 + b}{cV_1 + d}\right) = 0 \\
 \Rightarrow 1 + \frac{a}{cV_1 + d} - \frac{caV_1 + cb}{(cV_1 + d)^2} &= 0 \tag{3.18} \\
 \left\{ \begin{array}{l} a = A_2(\gamma mg + \gamma A_2 P_a - 4f_{\min}^2 \pi^2 m H_{eq}) \\ b = A_2 \gamma P_a A_1^2 H_{eq} + A_1 A_2 (H - H_{eq})(\gamma mg + \gamma A_2 P_a - 4f_{\min}^2 \pi^2 m H_{eq}) \\ c = 4f_{\min}^2 \pi^2 m \\ d = 4f_{\min}^2 \pi^2 m A_1 (H - H_{eq}) - \gamma P_a A_1^2 \end{array} \right.
 \end{aligned}$$

By solving this equation, the optimum values of V_1 and V_2 are:

$$\begin{aligned}
 V_{1-\min} &= \frac{\gamma P_a A_1^2 - 4f_{\min}^2 \pi^2 m A_1 (H - H_{eq}) + A_1 \sqrt{A_2 \gamma^2 P_a (mg + A_2 P_a)}}{4f_{\min}^2 \pi^2 m} \\
 V_{2-\min} &= \frac{A_1 A_2 \gamma^2 P_a (mg + A_2 P_a)}{4f_{\min}^2 \pi^2 m \sqrt{A_2 \gamma^2 P_a (mg + A_2 P_a)}} + \frac{A_2 \gamma (mg + A_2 P_a) - 4f_{\min}^2 \pi^2 m A_1 A_2 H_{eq}}{4f_{\min}^2 \pi^2 m} \tag{3.19}
 \end{aligned}$$

However, there is no guarantee that the optimum point will be above the intersection of minimum and maximum natural frequency curves (acceptable region). In cases, when the optimum point is below the intersection, the optimum answer is the intersection of the curves, which is:

$$\begin{aligned}
V_{1-int} &= \frac{A_1(4P_{max}A_2f_{min}^2\pi^2m(H-H_{eq}) - A_1A_2\gamma P_{max}P_a - (4f_{max}^2\pi^2m(H-H_{eq}) + \gamma(A_{damper}P_a - A_2P_{max} + mg))(mg + A_2P_a))}{4\pi^2m(f_{max}^2(mg + A_2P_a) - P_{max}A_2f_{min}^2)} \\
V_{2-int} &= \frac{-A_2((4f_{min}^2\pi^2mH_{eq} - \gamma(mg + A_2P_a))(mg + A_{damper}P_a - A_2P_{max}) - A_1A_2\gamma P_{max}P_a + 4f_{max}^2\pi^2mH_{eq}A_1P_a)}{4\pi^2m(f_{min}^2(mg + A_{damper}P_a - A_2P_{max}) - P_aA_1f_{max}^2)}
\end{aligned} \tag{3.20}$$

To conclude, it can be said that the optimum accumulators' volume are:

$$\begin{aligned}
V_{1-opt} &= \min(V_{1-min}, V_{1-int}) \\
V_{2-opt} &= \frac{aV_{1-opt} + b}{cV_{1-opt} + d} \rightarrow \begin{cases} a = A_2(\gamma mg + \gamma A_2P_a - 4f_{min}^2\pi^2mH_{eq}) \\ b = A_2\gamma P_aA_1^2H_{eq} + A_1A_2(H - H_{eq})(\gamma mg + \gamma A_2P_a - 4f_{min}^2\pi^2mH_{eq}) \\ c = 4f_{min}^2\pi^2m \\ d = 4f_{min}^2\pi^2mA_1(H - H_{eq}) - \gamma P_aA_1^2 \end{cases} \tag{3.21}
\end{aligned}$$

3.4 Determining the Cylinder Area and Damper Area

By assigning different cylinder area for cylinder and damper, different optimum accumulators' volume are found with considering all the design criteria. Therefore, the optimum areas should be selected to have the least accumulators' volume.

The basic constraints for areas are:

$$A_{Cylinder} = A_2 \leq \frac{\pi}{4} D_{Coil-Spring}^2 \quad \frac{\pi}{4} D_{Damper}^2 \leq A_{damper} \leq A_{Cylinder} \tag{3.22}$$

By plotting the $(V_1 + V_2)$ versus the A_2 and finding the minimum accumulators' volume, the optimum cylinder area can be found. Also, in the same by finding the minimum accumulators' volume on the $(V_1 + V_2)$ versus A_{damper} plot, the best choice for damper area will be found.

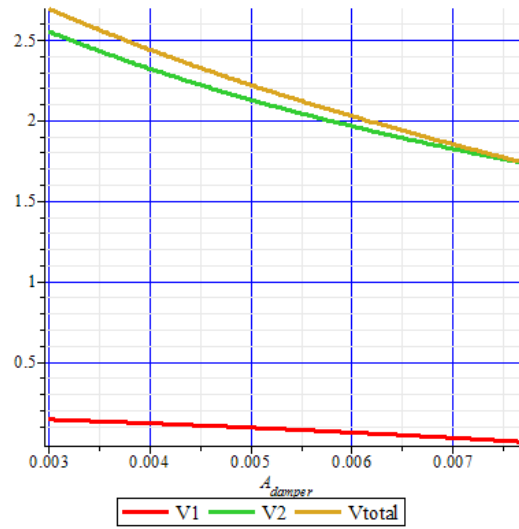


Figure 10- Accumulators' volume versus damper area

Figure 10 reveals that the maximum feasible damper area would be the best choice to have the minimum accumulators' volume. Based on the force equilibrium equation for system at the maximum working pressure in both chambers (increasing the damper area results in pressure increase at both chambers):

$$F_{(at\ z=H_{eq})} = mg \xrightarrow{P_{eq1}=P_{eq2}=P_{max}} A_{damper-max} = \frac{mg}{P_{max} - P_a} \quad (3.23)$$

Therefore, the boundaries for the feasible damper area are:

$$\frac{\pi}{4} D_{Damper}^2 \leq A_{damper} \leq A_{damper-max} = \frac{mg}{P_{max} - P_a} \quad (3.24)$$

3.5 Behavior of Air suspension During Extension and Compression

As aforementioned, the stiffness of air suspension system is a function of height. This means that by extension or compression, the height of the piston within the cylinder changes, and therefore the stiffness of the system would also be changed. This thesis prefers to find and monitor the natural frequency of air suspension instead of stiffness.

The natural frequency function is:

$$\left\{ \begin{array}{l} f_{(at\ any\ z)} = f(z) = \sqrt{\frac{\frac{P_2(z)\gamma A_2^2}{V_2 + A_2 z} + \frac{P_1(z)\gamma A_1^2}{V_1 + A_1(H - z)}}{m}} \\ P_1(z) = P_{eq1} \left(\frac{V_1 + A_1(H - H_{eq})}{V_1 + A_1(H - z)} \right)^\gamma \\ P_2(z) = P_{eq2} \left(\frac{V_2 + A_2 H_{eq}}{V_2 + A_2 z} \right)^\gamma \end{array} \right. \Rightarrow \quad (3.25)$$

$$f(z) = \sqrt{\frac{\frac{P_{eq2}(V_2 + A_2 H_{eq})^\gamma \gamma A_2^2}{(V_2 + A_2 z)^{\gamma+1}} + \frac{P_{eq1}(V_1 + A_1(H - H_{eq}))^\gamma \gamma A_1^2}{(V_1 + A_1(H - z))^{\gamma+1}}}{m}}$$

Moreover, the minimum natural frequency of the system based on the atmospheric pressure at the upper chamber is:

$$\left\{ \begin{array}{l} f_{\min}(z) = \sqrt{\frac{\frac{P_{2\min}(z)\gamma A_2^2}{V_2 + A_2 z} + \frac{P_{1\min}(z)\gamma A_1^2}{V_1 + A_1(H - z)}}{m}} \\ P_{1\min}(z) = P_a \left(\frac{V_1 + A_1(H - H_{eq})}{V_1 + A_1(H - z)} \right)^\gamma \\ P_{2\min}(z) = \left(\frac{mg + A_2 P}{A_2} \right) \left(\frac{V_2 + A_2 H_{eq}}{V_2 + A_2 z} \right)^\gamma \end{array} \right. \Rightarrow \quad (3.26)$$

$$f_{\min}(z) = \sqrt{\frac{\frac{(mg + A_2 P)(V_2 + A_2 H_{eq})^\gamma \gamma A_2^2}{(V_2 + A_2 z)^{\gamma+1}} + \frac{P_a (V_1 + A_1(H - H_{eq}))^\gamma \gamma A_1^2}{(V_1 + A_1(H - z))^{\gamma+1}}}{m}}$$

The maximum natural frequency based on the maximum working pressure at the lower chamber is:

$$\left\{ \begin{array}{l}
f_{\max}(z) = \sqrt{\frac{\frac{P_{2\max}(z)\gamma A_2^2}{V_2 + A_2 z} + \frac{P_{1\max}(z)\gamma A_1^2}{V_1 + A_1(H-z)}}{m}} \\
P_{1\max}(z) = \left(\frac{P_{\max} A_2 - P_a A_{damp} - mg}{A_1} \right) \left(\frac{V_1 + A_1(H - H_{eq})}{V_1 + A_1(H - z)} \right)^\gamma \\
P_{2\max}(z) = P_{\max} \left(\frac{V_2 + A_2 H_{eq}}{V_2 + A_2 z} \right)^\gamma
\end{array} \right. \Rightarrow \quad (3.27)$$

$$f_{\max}(z) = \sqrt{\frac{\frac{P_{\max} (V_2 + A_2 H_{eq})^\gamma \gamma A_2^2}{(V_2 + A_2 z)^{\gamma+1}} + \frac{(P_{\max} A_2 - P_a A_{damp} - mg)(V_1 + A_1(H - H_{eq}))^\gamma \gamma A_1}{(V_1 + A_1(H - z))^{\gamma+1}}}{m}}$$

By plotting the natural frequency functions versus the suspension travel (z), the variation of stiffness at the full suspension stroke can be studied.

3.6 Extra Load

Suspension system is designed based on the nominal vehicle mass, which includes the net mass of the vehicle plus half of the maximum allowed load of the vehicle. In the worst case scenario, which is the maximum load situation, the effect of the extra load on the behavior of the air suspension should be studied. Obviously, after adding extra load, the piston moves down and will not be in the desired equilibrium position (without controller to set the pressure of chambers to reach the desired equilibrium position). Extra load situation is a permanent change in the system for a while, and gas has enough time to transfer heat. Therefore, the gas temperature can reach its initial temperature. Since, the isothermal process will be considered, the behavior of air suspension is:

$$\begin{aligned}
PV &= C \Rightarrow P = \frac{C}{V} \\
P_1(z) &= \frac{C_1}{V_1 + A_1(H - z)} \quad P_2(z) = \frac{C_2}{V_2 + A_2z} \\
F(z) &= \left(\frac{C_2}{V_2 + A_2z} - P_a \right) A_2 - \left(\frac{C_1}{V_1 + A_1(H - z)} - P_a \right) A_1
\end{aligned} \tag{3.28}$$

and the stiffness becomes:

$$K = -\frac{\partial F}{\partial z} = \frac{C_2 A_2^2}{V_2 + A_2z} + \frac{C_1 A_1^2}{V_1 + A_1(H - z)} = \frac{P_2(z) A_2^2}{V_2 + A_2z} + \frac{P_1(z) A_1^2}{V_1 + A_1(H - z)} \tag{3.29}$$

Also, the natural frequency of suspension is defined:

$$f = \frac{\sqrt{\frac{P_2(z) A_2^2}{V_2 + A_2z} + \frac{P_1(z) A_1^2}{V_1 + A_1(H - z)}}}{2\pi} \tag{3.30}$$

The natural frequency of the system for isothermal and isentropic process are:

$$f_{Isentropic} = \sqrt{\gamma} f_{Isothermal} \Rightarrow f_{Isothermal} = 0.845 f_{Isentropic} \tag{3.31}$$

where γ is the heat capacity ratio of gas. For instance, the isothermal natural frequency of air suspension is 1.05 Hz at the equilibrium position where the isentropic natural frequency is 1.25 Hz.

The force equilibrium equation should be satisfied after adding extra load:

$$\begin{cases}
F_{(at\ z=H_{eq})} = mg \Rightarrow mg = (P_{eq2} - P_a) A_2 - (P_{eq1} - P_a) A_1 \\
F_{(at\ z=H_{eq-new})} = (m + m_l) g \Rightarrow (m + m_l) g = (P_{eq2-new} - P_a) A_2 - (P_{eq1-new} - P_a) A_1
\end{cases} \tag{3.32}$$

where m_l is extra load mass and $H_{eq} > H_{eq-new}$. $P_{eq2-new}$ and $P_{eq1-new}$ are the new equilibrium pressure of chambers based on the isothermal process:

$$P_{eq1-new} = \frac{P_{eq1}(V_1 + A_1(H - H_{eq}))}{V_1 + A_1(H - H_{eq-new})} \quad P_{eq2-new} = \frac{P_{eq2}(V_2 + A_2 H_{eq})}{V_2 + A_2 H_{eq-new}} \tag{3.33}$$

By subtracting the force equilibrium equations:

$$m_l g = (H_{eq} - H_{eq-new}) \frac{P_{eq2} A_2^2}{V_2 + A_2 H_{eq-new}} + \frac{P_{eq1} A_1^2}{V_1 + A_1 (H - H_{eq-new})} \quad (3.34)$$

The new equilibrium position would be:

$$H_{eq-new} = \frac{b - \sqrt{b^2 - 4ac}}{2a} \rightarrow \quad (3.35)$$

$$\begin{cases} a = P_{eq2} A_2^2 A_1 - P_{eq1} A_1^2 A_2 + m_l g A_2 A_1 \\ b = P_{eq1} A_1^2 (A_2 H_{eq} - V_2) - P_{eq2} A_2^2 (V_1 + A_1 (H + H_{eq})) + (m_l g (A_1 V_2 - A_2 V_1 - A_2 A_1 H)) \\ c = P_{eq2} A_2 H_{eq} (V_1 A_2 + A_1 A_2 H) + P_{eq1} A_1^2 H_{eq} V_2 - m_l g V_2 (V_1 + A_1 H) \end{cases}$$

The deflection of suspension due to extra load should be calculated based on the isothermal process; after finding the new equilibrium position, the system works again based on the isentropic process. On the other hand, the pressure of the chambers can be set by the controller to have the same initial equilibrium position.

3.7 Ride Height Tuning

The other advantage of this air suspension system is ride height tuning. It is possible to achieve the same desired natural frequency in different equilibrium height (ride height), by changing the equilibrium pressure of chambers. Tuning the equilibrium height changes the initial volume of chambers and the natural frequency will change as well. Therefore, the pressures should be set to reach the same natural frequency as before. The new equilibrium pressures for a new ride height are a function of equilibrium height:

$$\begin{aligned}
P_{eq1} &= \left(\frac{a}{d_1}\right) H_{eq}^2 + \left(\frac{b}{d_1}\right) H_{eq} + \left(\frac{c_1}{d_1}\right) & P_{eq2} &= \left(\frac{a}{d_2}\right) H_{eq}^2 + \left(\frac{b}{d_2}\right) H_{eq} + \left(\frac{c_2}{d_2}\right) \\
\left\{ \begin{array}{l} a = 4f_s^2 \pi^2 m A_1 A_2 \\ b = 4f_s^2 \pi^2 m (A_2 (A_1 H + V_1) - V_2 A_1) + A_1 A_2 \gamma (A_{damper} P_a + mg) \\ c_1 = (4f_s^2 \pi^2 m V_2 - A_2 \gamma (A_{damper} P_a + mg)) (V_1 + A_1 H) \\ d_1 = A_1 \gamma (A_1 V_2 + A_2 V_1 + A_1 A_2 H) \end{array} \right. & & (3.36) \\
\left\{ \begin{array}{l} c_2 = V_2 (4f_s^2 \pi^2 m (V_1 + A_1 H) + A_1 \gamma (A_{damper} P_a + mg)) \\ d_2 = A_2 \gamma (A_1 V_2 + A_2 V_1 + A_1 A_2 H) \end{array} \right.
\end{aligned}$$

3.8 Numerical Solutions

A computer code can check all the V_1 and V_2 in a reasonable range of accumulators' volume. This code for each couple of V_1 and V_2 does the following procedure: Firstly, it calculates the equilibrium pressures and then checks the minimum pressure constraint, both of them (upper and lower chambers pressures) should be greater than the atmospheric pressure. Secondly, the program calculates the maximum and minimum natural frequencies based on the available maximum and minimum pressures of the system. After that, it is checked whether these maximum and minimum natural frequencies can cover the desired range of natural frequency or not. If the answer is yes, this couple of V_1 and V_2 will be saved as one of the accepted answers but not the optimum. By searching between all of the accumulators' volume, the possible solutions will be determined as shown in Figure 11.

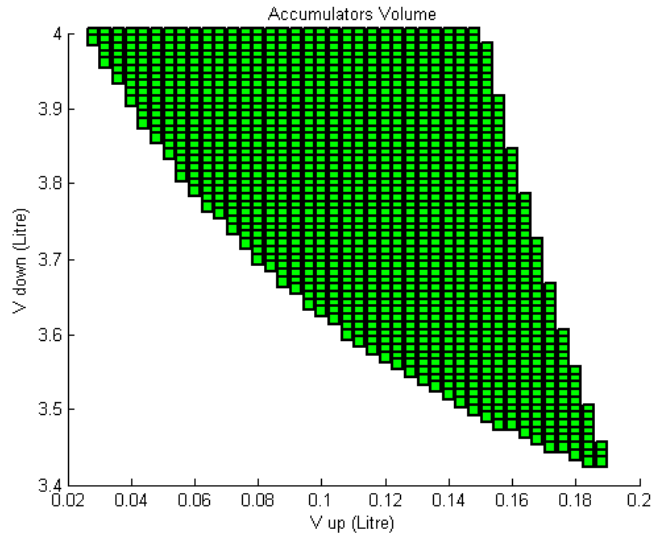


Figure 11- possible solutions for accumulators' volume

And lastly, the program finds the minimum ($V_1 + V_2$) as a final optimum solution for the accumulators' volume. These volumes are same as the results from an analytical solution.

Chapter 4 Effect of Interconnected Air Suspensions on Vehicle Performance

The interconnection between the pressurized chambers of the air suspension with ride height and stiffness tuning, is studied to further improve the new air suspension performance. Proper interconnection of air springs can help the suspension system distribute the load between tires more evenly on rough roads and also, reduce transmitted vibration to the vehicle body. This chapter focuses on the analysis of different interconnection configurations. Moreover, interconnection of air springs has a better impact on the performance of the vehicle with three or more axles in heavy vehicles. Therefore, the general mathematical model is developed for a heavy truck with a three-axle configuration.

4.1 System Modeling with an Independent Air Suspensions

As shown in Figure 12, the model has nine degrees of freedom. Three DOF for sprung mass (M_s): bounce, pitch, and roll and six DOF for vertical motion of unsprung masses (M_u). L_f , L_m , and L_b are the distance of front, first rear, and second rear axles from the CG, respectively. Z_s , θ , and ϕ show the bounce, pitch, and roll motion of sprung mass. Each tire has one input, which is road profile (Z_g), and one DOF which is unsprung mass motion (Z_u).

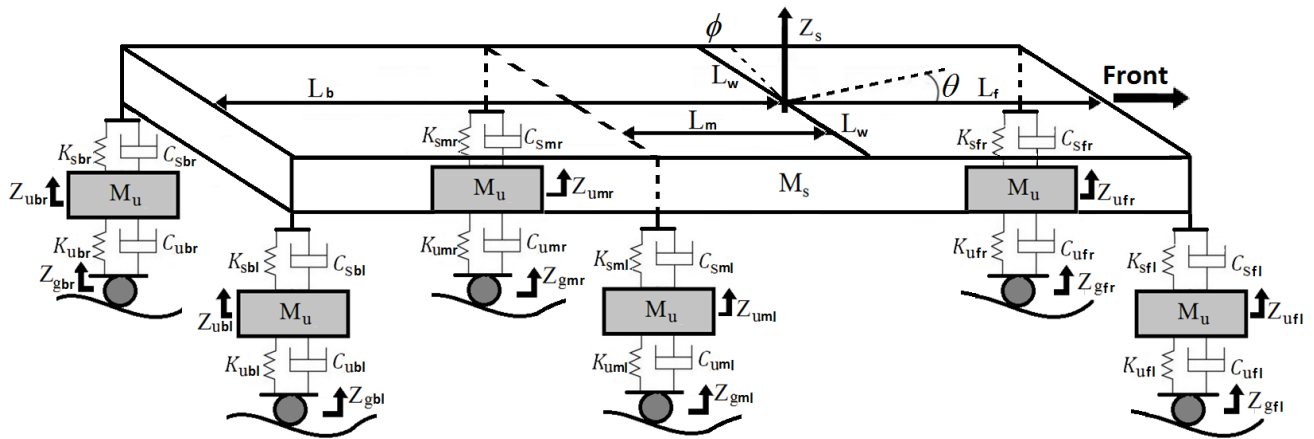


Figure 12- Truck model with three axles

Considering the fact that the suspension systems are air suspension with ride height and stiffness tuning, the general diagram of air spring is one of the following types shown in Figure 13.

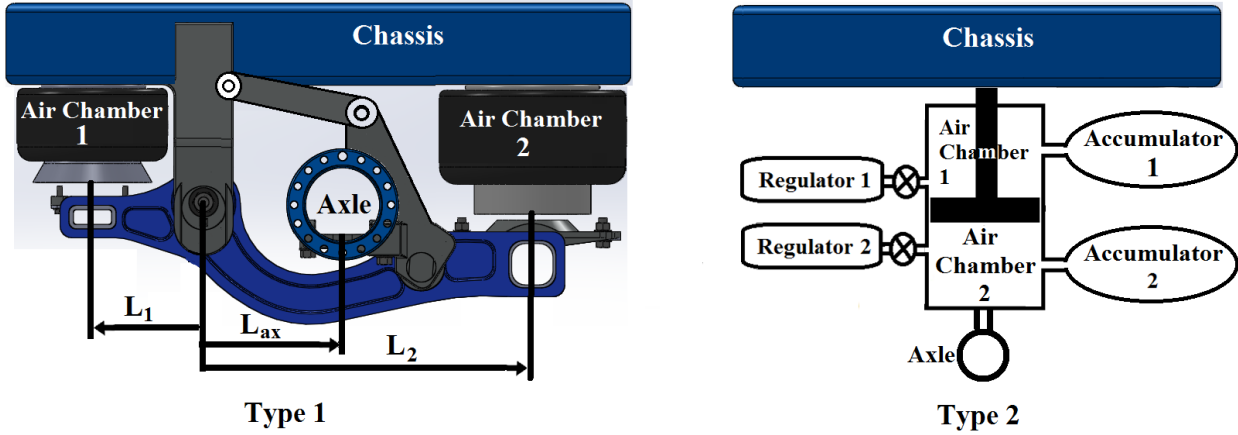


Figure 13- different types of pneumatic spring

The equivalent stiffness at axle point for type 1 is:

$$\frac{L_1}{L_{ax}} = a \quad \frac{L_2}{L_{ax}} = b \quad (4.1)$$

$$K_{eq} = a^2 K_1 + b^2 K_2$$

where K_1 and K_2 are stiffness of air springs or air chamber 1 and 2 respectively. L_1 and L_2 are distances of air chamber 1 and 2 from pivot point, respectively. L_{ax} is the effective distances of axle from pivot point, which is calculated based on four-bar linkage equations (Appendix 1) and also, a and b are the length ratios of air chamber 1 and 2, respectively.

Since, in type 2 the air chambers are exactly at the top of the axle point. Therefore, the length ratios are:

$$a = 1 \quad b = 1 \quad (4.2)$$

$$K_{eq} = K_1 + K_2$$

The state space equation of the system is defined based on the dynamic equations for sprung and unsprung masses. For simplicity, it can be assumed that the front suspensions have same

tires, springs, and dampers and also all the rear suspensions have the same:

$$\begin{aligned}
K_{sfr} = K_{sfl} = K_{sf} = a_f^2 K_{sf1} + b_f^2 K_{sf2} & & K_{smr} = K_{sml} = K_{sbr} = K_{sbl} = K_{sr} = a_r^2 K_{sr1} + b_r^2 K_{sr2} \\
K_{ufr} = K_{ufl} = K_{uf} & & K_{tm} = K_{tb} = K_{tr} \\
C_{sfr} = C_{sfl} = C_{sf} & & K_{umr} = K_{uml} = K_{ubr} = K_{ubl} = K_{ur} \\
C_{ufr} = C_{ufl} = C_{uf} & & C_{smr} = C_{sml} = C_{sbr} = C_{sbl} = C_{sr} \\
& & C_{umr} = C_{uml} = C_{ubr} = C_{ubl} = C_{ur}
\end{aligned} \tag{4.3}$$

where a_f and b_f are length ratios of air chambers for front suspensions. And also, a_r and b_r are length ratios of rear suspensions.

The state space of system is:

$$\begin{aligned}
\dot{X} &= \underbrace{\begin{bmatrix} A_{C-\min} 9 \times 9 & A_{K-\min} 9 \times 9 \\ I_{9 \times 9} & 0_{9 \times 9} \end{bmatrix}}_{A_{18 \times 18}} X + \underbrace{\begin{bmatrix} 0_{3 \times 12} \\ B_{C-\min} 6 \times 6 & B_{K-\min} 6 \times 6 \\ 0_{9 \times 12} \end{bmatrix}}_{B_{18 \times 12}} U \\
Y &= \underbrace{\begin{bmatrix} 0_{6 \times 3} & C_{C-\min} 6 \times 6 & 0_{6 \times 3} & C_{K-\min} 6 \times 6 \end{bmatrix}}_{C_{6 \times 18}} X + \underbrace{\begin{bmatrix} D_{C-\min} 6 \times 6 & D_{K-\min} 6 \times 6 \end{bmatrix}}_{D_{6 \times 12}} U \\
\dot{X} &= \left[\ddot{Z}_s \quad \ddot{\theta} \quad \ddot{\phi} \quad \ddot{Z}_{ufr} \quad \ddot{Z}_{ufl} \quad \ddot{Z}_{umr} \quad \ddot{Z}_{uml} \quad \ddot{Z}_{ubr} \quad \ddot{Z}_{ubl} \quad \dot{Z}_s \quad \dot{\theta} \quad \dot{\phi} \quad \dot{Z}_{ufr} \quad \dot{Z}_{ufl} \quad \dot{Z}_{umr} \quad \dot{Z}_{uml} \quad \dot{Z}_{ubr} \quad \dot{Z}_{ubl} \right]^T \\
X &= \left[\dot{Z}_s \quad \dot{\theta} \quad \dot{\phi} \quad \dot{Z}_{ufr} \quad \dot{Z}_{ufl} \quad \dot{Z}_{umr} \quad \dot{Z}_{uml} \quad \dot{Z}_{ubr} \quad \dot{Z}_{ubl} \quad Z_s \quad \theta \quad \phi \quad Z_{ufr} \quad Z_{ufl} \quad Z_{umr} \quad Z_{uml} \quad Z_{ubr} \quad Z_{ubl} \right]^T \\
U &= \left[\dot{Z}_{gfr} \quad \dot{Z}_{gfl} \quad \dot{Z}_{gmr} \quad \dot{Z}_{gml} \quad \dot{Z}_{gbr} \quad \dot{Z}_{gbl} \quad Z_{gfr} \quad Z_{gfl} \quad Z_{gmr} \quad Z_{gml} \quad Z_{gbr} \quad Z_{gbl} \right]^T \\
Y &= \left[F_{gfr} \quad F_{gfl} \quad F_{gmr} \quad F_{gml} \quad F_{gbr} \quad F_{gbl} \right]^T
\end{aligned} \tag{4.4}$$

where, F_g is the tire force. It has been defined based on the tire deflection times the tire stiffness, plus the derivative of tire deflection time by the damping coefficient of tire. Normally it is assumed that the damping coefficient of the tire is zero. However, the general format of sub-matrixes are:

$$\begin{aligned}
m_u [B_{C-\min \ 6 \times 6}] &= [D_{C-\min \ 6 \times 6}] = -[C_{C-\min \ 6 \times 6}] = \begin{bmatrix} C_{uf} & 0 & 0 & 0 & 0 & 0 \\ 0 & C_{uf} & 0 & 0 & 0 & 0 \\ 0 & 0 & C_{ur} & 0 & 0 & 0 \\ 0 & 0 & 0 & C_{ur} & 0 & 0 \\ 0 & 0 & 0 & 0 & C_{ur} & 0 \\ 0 & 0 & 0 & 0 & 0 & C_{ur} \end{bmatrix} \\
m_u [B_{K-\min \ 6 \times 6}] &= [D_{K-\min \ 6 \times 6}] = -[C_{K-\min \ 6 \times 6}] = \begin{bmatrix} K_{uf} & 0 & 0 & 0 & 0 & 0 \\ 0 & K_{uf} & 0 & 0 & 0 & 0 \\ 0 & 0 & K_{ur} & 0 & 0 & 0 \\ 0 & 0 & 0 & K_{ur} & 0 & 0 \\ 0 & 0 & 0 & 0 & K_{ur} & 0 \\ 0 & 0 & 0 & 0 & 0 & K_{ur} \end{bmatrix}
\end{aligned} \tag{4.5}$$

$$[A_{C-\min 9 \times 9}] = \begin{bmatrix} -C_s M_s^{-1} & -C_1 M_s^{-1} & 0 & C_{sf} M_s^{-1} & C_{sf} M_s^{-1} & C_{sr} M_s^{-1} & C_{sr} M_s^{-1} & C_{sr} M_s^{-1} & C_{sr} M_s^{-1} \\ -C_1 I_{sy}^{-1} & -C_2 I_{sy}^{-1} & 0 & L_f C_{sf} I_{sy}^{-1} & L_f C_{sf} I_{sy}^{-1} & -L_m C_{sr} I_{sy}^{-1} & -L_m C_{sr} I_{sy}^{-1} & -L_b C_{sr} I_{sy}^{-1} & -L_b C_{sr} I_{sy}^{-1} \\ 0 & 0 & -L_w^2 C_s I_{sx}^{-1} & L_w C_{sf} I_{sx}^{-1} & -L_w C_{sf} I_{sx}^{-1} & L_w C_{sr} I_{sx}^{-1} & -L_w C_{sr} I_{sx}^{-1} & L_w C_{sr} I_{sx}^{-1} & -L_w C_{sr} I_{sx}^{-1} \\ C_{sf} m_u^{-1} & L_f C_{sf} m_u^{-1} & L_w C_{sf} m_u^{-1} & \frac{-C_{sf} - C_{uf}}{m_u} & 0 & 0 & 0 & 0 & 0 \\ C_{sf} m_u^{-1} & L_f C_{sf} m_u^{-1} & -L_w C_{sf} m_u^{-1} & 0 & \frac{-C_{sf} - C_{uf}}{m_u} & 0 & 0 & 0 & 0 \\ 0 & C_{sr} m_u^{-1} & -L_m C_{sr} m_u^{-1} & L_w C_{sr} m_u^{-1} & 0 & 0 & \frac{-C_{sr} - C_{ur}}{m_u} & 0 & 0 \\ C_{sr} m_u^{-1} & -L_m C_{sfl} m_u^{-1} & -L_w C_{sr} m_u^{-1} & 0 & 0 & 0 & \frac{-C_{sr} - C_{ur}}{m_u} & 0 & 0 \\ C_{sr} m_u^{-1} & -L_b C_{sr1l} m_u^{-1} & L_w C_{sr} m_u^{-1} & 0 & 0 & 0 & 0 & \frac{-C_{sr} - C_{ur}}{m_u} & 0 \\ C_{sr} m_u^{-1} & -L_b C_{sr2l} m_u^{-1} & -L_w C_{sr} m_u^{-1} & 0 & 0 & 0 & 0 & 0 & \frac{-C_{sr} - C_{ur}}{m_u} \end{bmatrix}$$

$$C_s = 2C_{sf} + 4C_{sr}$$

$$C_1 = 2L_f C_{sf} - 2(L_m + L_b)C_{sr}$$

$$C_2 = 2L_f^2 C_{sf} + 2(L_m^2 + L_b^2)C_{sr}$$

(4.6)

$$[A_{K-\min} 9 \times 9] = \begin{bmatrix} -K_s M_s^{-1} & -K_1 M_s^{-1} & 0 & K_{sf} M_s^{-1} & K_{sf} M_s^{-1} & K_{sr} M_s^{-1} & K_{sr} M_s^{-1} & K_{sr} M_s^{-1} & K_{sr} M_s^{-1} \\ -K_1 I_{sy}^{-1} & -K_2 I_{sy}^{-1} & 0 & L_f K_{sf} I_{sy}^{-1} & L_f K_{sf} I_{sy}^{-1} & -L_m K_{sr} I_{sy}^{-1} & -L_m K_{sr} I_{sy}^{-1} & -L_b K_{sr} I_{sy}^{-1} & -L_b K_{sr} I_{sy}^{-1} \\ 0 & 0 & -\frac{L_w^2 K_3}{I_{sx}} & \frac{L_w^2 K_{sf} + K_{tff}}{I_{sx} L_w} & \frac{L_w^2 K_{sf} + K_{tff}}{I_{sx} L_w} & \frac{L_w^2 K_{sr} + K_{trr}}{I_{sx} L_w} \\ K_{sf} m_u^{-1} & L_f K_{sf} m_u^{-1} & \frac{L_w K_{sf} + K_{tff}}{m_u} & \frac{-K_{sf} - K_{tff}}{m_u} & 0 & 0 & 0 & 0 & 0 \\ K_{sf} m_u^{-1} & L_f K_{sf} m_u^{-1} & -\frac{L_w K_{sf} + K_{tff}}{m_u} & 0 & \frac{-K_{sf} - K_{tff}}{m_u} & 0 & 0 & 0 & 0 \\ K_{sr} m_u^{-1} & -L_m K_{sr} m_u^{-1} & \frac{L_w K_{sr} + K_{trr}}{m_u} & 0 & 0 & \frac{-K_{sr} - K_{trr}}{m_u} & 0 & 0 & 0 \\ K_{sr} m_u^{-1} & -L_m K_{sfl} m_u^{-1} & -\frac{L_w K_{sr} + K_{trr}}{m_u} & 0 & 0 & 0 & \frac{-K_{sr} - K_{trr}}{m_u} & 0 & 0 \\ K_{sr} m_u^{-1} & -L_b K_{sr1l} m_u^{-1} & \frac{L_w K_{sr} + K_{trr}}{m_u} & 0 & 0 & 0 & 0 & \frac{-K_{sr} - K_{trr}}{m_u} & 0 \\ K_{sr} m_u^{-1} & -L_b K_{sr2l} m_u^{-1} & -\frac{L_w K_{sr} + K_{trr}}{m_u} & 0 & 0 & 0 & 0 & 0 & \frac{-K_{sr} - K_{trr}}{m_u} \end{bmatrix}$$

$$K_1 = 2L_f K_{sf} - 2(L_m + L_b) K_{sr}$$

$$K_s = 2K_{sf} + 4K_{sr}$$

$$K_2 = 2L_f^2 K_{sf} + 2(L_m^2 + L_b^2) K_{sr}$$

$$K_3 = 2K_{sf} + 4K_{sr} + \frac{K_{tff} + 2K_{trr}}{L_w^2}$$

$$K_{tff} = K_{tff} (2L_w)^{-1}$$

$$K_{trr} = K_{trr} (2L_w)^{-1}$$

(4.7)

4.2 Interconnected Air Chambers

The gas inside the independent air chamber shown in Figure 14, behaves based on the isentropic process:

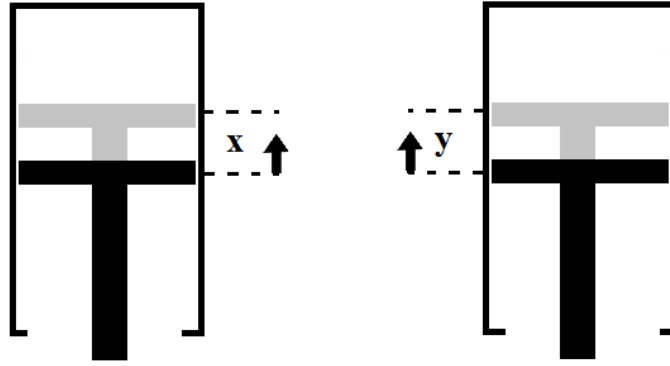


Figure 14- Independent air chambers

$$\begin{aligned}
 PV^\gamma &= C \Rightarrow P = \frac{C}{V^\gamma} \\
 P(x) &= \frac{P_0 V_0^\gamma}{(V_0 - Ax)^\gamma} \Rightarrow F(x) = \frac{AP_0 V_0^\gamma}{(V_0 - Ax)^\gamma} \\
 P(y) &= \frac{P_0 V_0^\gamma}{(V_0 - Ay)^\gamma} \Rightarrow F(y) = \frac{AP_0 V_0^\gamma}{(V_0 - Ay)^\gamma}
 \end{aligned} \tag{4.8}$$

When chambers are connected as shown in Figure 15, the pressure in both chambers is identical. This assumption would be valid when the connecting pipes and fittings do not have any pressure loss.

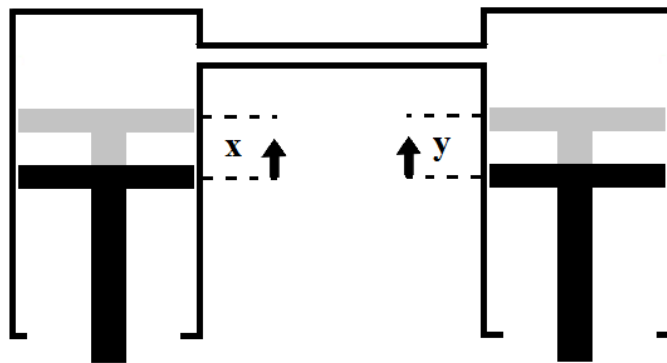


Figure 15- Connected air chambers

Therefore, the behavior of system can be described with the isentropic formula for the volume of gas in both air chambers.

$$P(x, y)(2V_0 - Ax - Ay)^\gamma = P_0(2V_0)^\gamma$$

$$F(x, y) = \frac{AP_0(2V_0)^\gamma}{(2V_0 - Ax - Ay)^\gamma} = \frac{AP_0V_0^\gamma}{\left(V_0 - A\left(\frac{x+y}{2}\right)\right)^\gamma} \quad (4.9)$$

If it is assumed that the stiffness of air chamber is constant and K , then, for two connected chambers, force formula is:

$$F_{air-chamber} = F(x, y) = K\left(\frac{x+y}{2}\right) \quad (4.10)$$

This equation shows that the force exerted by each air chamber is equal to the stiffness times by the average displacement of connected air chambers from the equilibrium point. This conclusion can be generalized for any number of connected air chambers.

$$F_{air-chamber} = F(x_1, x_2, \dots, x_n) = K\left(\frac{x_1 + x_2 + \dots + x_n}{n}\right) \quad (4.11)$$

To show the general format for studying the different configurations of interconnection, connection indexes is proposed.

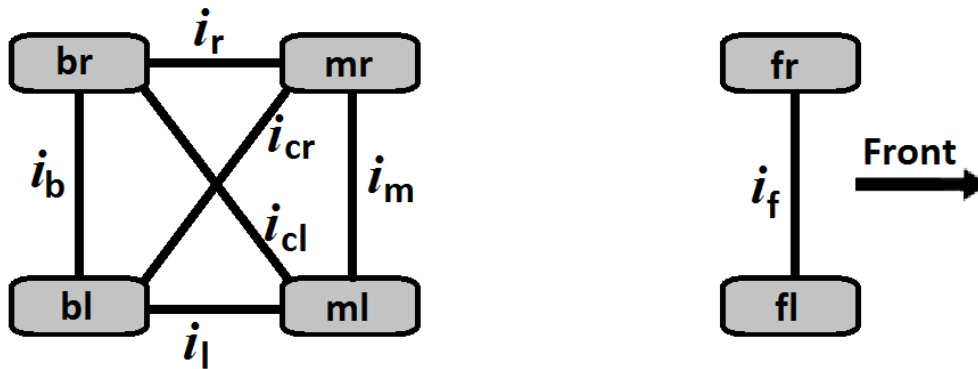


Figure 16- Top view of truck and interconnection indexes

As Figure 16 shows, black lines with i shows the possible connections between air chambers. When i is zero, it means that there is no interconnection and when i is one, it means that those air

chambers are connected to each other. These are connection indexes between one set of chambers (air chamber 1 or 2) from each air suspension systems. For the other set of air chambers, the same notation will be used.

By substituting the new formula for connected air chambers and considering the notation for interconnection in the dynamic equations, the new state space form of the system is extracted, which is similar to the original system. The only difference is some changes in quarter sub-matrix related to the spring stiffness in A matrix ($A_{K-\min\ 9\times9}$). The new sub-matrix for stiffness includes two matrixes. The first matrix ($A_{K-\min-IntCon-1}$) is related to the stiffness of interconnected air chamber 1 as shown in Figure 13 and the second one is about interconnected air chamber 2.

$$\begin{aligned}
 \dot{X} &= \underbrace{\begin{bmatrix} A_{C-\min\ 9\times9} & A_{K-\min\ IntCon-1} + A_{K-\min\ IntCon-2} \\ I_{9\times9} & 0_{9\times9} \end{bmatrix}}_{A_{18\times18}} X + \underbrace{\begin{bmatrix} 0_{3\times12} \\ B_{C-\min\ 6\times6} & B_{K-\min\ 6\times6} \\ 0_{9\times12} \end{bmatrix}}_{B_{18\times12}} U \\
 Y &= \underbrace{\begin{bmatrix} 0_{6\times3} & C_{C-\min\ 6\times6} & 0_{6\times3} & C_{K-\min\ 6\times6} \end{bmatrix}}_{C_{6\times18}} X + \underbrace{\begin{bmatrix} D_{C-\min\ 6\times6} & D_{K-\min\ 6\times6} \end{bmatrix}}_{D_{6\times12}} U \quad (4.12)
 \end{aligned}$$

$$\left[A_{K - \min}^{IntCon-1/2} \right]_{9 \times 9} = \begin{bmatrix}
-K_s M_s^{-1} & -K_1 M_s^{-1} & 0 & K_{sf} M_s^{-1} & K_{sf} M_s^{-1} & K_{sr} M_s^{-1} & K_{sr} M_s^{-1} & K_{sr} M_s^{-1} & K_{sr} M_s^{-1} \\
-K_1 I_{sy}^{-1} & -K_2 I_{sy}^{-1} & 0 & K_{sf} a_9 I_{sy}^{-1} & K_{sf} a_9 I_{sy}^{-1} & -K_{sr} a_1 I_{sy}^{-1} & -K_{sr} a_2 I_{sy}^{-1} & -K_{sr} a_3 I_{sy}^{-1} & -K_{sr} a_4 I_{sy}^{-1} \\
0 & 0 & -L_w^2 K_3 I_{sx}^{-1} & \frac{K_{sf} a_{10} + K_{tff}}{I_{sx}} & -\frac{K_{sf} a_{10} + K_{tff}}{I_{sx}} & \frac{K_{sr} a_5 + K_{ttr}}{I_{sx}} & -\frac{K_{sr} a_6 + K_{ttr}}{I_{sx}} & \frac{K_{sr} a_7 + K_{ttr}}{I_{sx}} & -\frac{K_{sr} a_8 + K_{ttr}}{I_{sx}} \\
\frac{K_{sf}}{m_u} & \frac{K_{sf} a_9}{m_u} & \frac{K_{sf} a_{10} + K_{tff}}{m_u} & -K_{uf} - \frac{K_{sf}}{1+i_f} & -\frac{i_f K_{sf}}{m_u (1+i_f)} & 0 & 0 & 0 & 0 \\
\frac{K_{sf}}{m_u} & \frac{K_{sf} a_9}{m_u} & -\frac{K_{sf} a_{10} + K_{tff}}{m_u} & -\frac{i_f K_{sf}}{m_u (1+i_f)} & \frac{-K_{uf} - \frac{K_{sf}}{1+i_f}}{m_u} & 0 & 0 & 0 & 0 \\
\frac{K_{sr}}{m_u} & -\frac{K_{sr} a_1}{m_u} & \frac{K_{sr} a_5 + K_{ttr}}{m_u} & 0 & 0 & \frac{-K_{ur} - \frac{K_{sr}}{a_{11}}}{m_u} & -\frac{i_m K_{sr}}{m_u a_{12}} & -\frac{i_r K_{sr}}{m_u a_{13}} & -\frac{i_{cr} K_{sr}}{m_u a_{14}} \\
\frac{K_{sr}}{m_u} & -\frac{K_{sr} a_2}{m_u} & -\frac{K_{sr} a_6 + K_{ttr}}{m_u} & 0 & 0 & -\frac{i_m K_{sr}}{m_u a_{11}} & \frac{-K_{ur} - \frac{K_{sr}}{a_{12}}}{m_u} & -\frac{i_{cl} K_{sr}}{m_u a_{13}} & -\frac{i_l K_{sr}}{m_u a_{14}} \\
\frac{K_{sr}}{m_u} & -\frac{K_{sr} a_3}{m_u} & \frac{K_{sr} a_7 + K_{ttr}}{m_u} & 0 & 0 & -\frac{i_r K_{sr}}{m_u a_{11}} & -\frac{i_{cl} K_{sr}}{m_u a_{12}} & \frac{-K_{ur} - \frac{K_{sr}}{a_{13}}}{m_u} & -\frac{i_b K_{sr}}{m_u a_{14}} \\
\frac{K_{sr}}{m_u} & -\frac{K_{sr} a_4}{m_u} & -\frac{K_{sr} a_8 + K_{ttr}}{m_u} & 0 & 0 & -\frac{i_{cr} K_{sr}}{m_u a_{11}} & -\frac{i_l K_{sr}}{m_u a_{12}} & -\frac{i_b K_{sr}}{m_u a_{13}} & \frac{-K_{ur} - \frac{K_{sr}}{a_{14}}}{m_u}
\end{bmatrix}$$

(4.13)

where,

$$\begin{aligned}
K_s &= 2K_{sf} + 4K_{sr} \\
K_1 &= 2L_f K_{sf} - 2(L_m + L_b)K_{sr} \\
K_2 &= 2L_f^2 K_{sf} + \left(2(L_m^2 + L_b^2) - (\text{sign}(i_r + i_l + i_{cr} + i_{cl}))(L_m - L_b)^2\right)K_{sr} \\
K_3 &= 2K_{sf}(1 - i_f) + 4K_{sr}(1 - \text{sign}(i_m + i_b + i_{cr} + i_{cl})) + \frac{K_{tf} + 2K_{tr}}{L_w^2} \\
K_{tf} &= \frac{K_{ff}}{2L_w} & K_{tr} &= \frac{K_{tr}}{2L_w} \\
a_1 &= \frac{L_m(1 + i_m) + L_b(i_r + i_{cr})}{1 + i_m + i_r + i_{cr}} & a_5 &= \frac{L_w(1 - i_m + i_r - i_{cr})}{1 + i_m + i_r + i_{cr}} \\
a_2 &= \frac{L_m(1 + i_m) + L_b(i_l + i_{cl})}{1 + i_m + i_l + i_{cl}} & a_6 &= \frac{L_w(1 - i_m + i_l - i_{cl})}{(1 + i_m + i_l + i_{cl})} \\
a_3 &= \frac{L_b(1 + i_b) + L_m(i_r + i_{cl})}{1 + i_b + i_r + i_{cl}} & a_7 &= \frac{L_w(1 - i_b + i_r - i_{cl})}{1 + i_b + i_r + i_{cl}} \\
a_4 &= \frac{L_b(1 + i_b) + L_m(i_l + i_{cr})}{1 + i_b + i_l + i_{cr}} & a_8 &= \frac{L_w(1 - i_b + i_l - i_{cr})}{1 + i_b + i_l + i_{cr}} \\
a_9 &= \frac{L_f(1 + i_f)}{1 + i_f} & a_{10} &= \frac{L_w(1 - i_f)}{1 + i_f} \\
a_{11} &= 1 + i_m + i_r + i_{cr} & a_{13} &= 1 + i_b + i_r + i_{cl} \\
a_{12} &= 1 + i_m + i_l + i_{cl} & a_{14} &= 1 + i_b + i_l + i_{cr}
\end{aligned} \tag{4.14}$$

As it mentioned, the general format of both stiffness sub-matrixes are the same, but each one is for the different set of air chambers:

$$\begin{aligned}
\left[\begin{array}{c} A_{K - \min} \\ IntCon-1 \end{array} \right] &\longrightarrow \begin{cases} K_{sf} = a_f^2 K_{sf1} \\ K_{sr} = a_r^2 K_{sr1} \end{cases} \\
\left[\begin{array}{c} A_{K - \min} \\ IntCon-2 \end{array} \right] &\longrightarrow \begin{cases} K_{sf} = b_f^2 K_{sf2} \\ K_{sr} = b_r^2 K_{sr2} \end{cases}
\end{aligned} \tag{4.15}$$

where a_f , b_f , and a_r , b_r , are length ratios for front and rear air suspensions respectively and also K_{sf1} , K_{sf2} , and K_{sr1} , K_{sr2} , are stiffness of each air chamber in front and rear air suspensions, respectively.

There are several configurations for the interconnection of rear air suspensions. Table 2 represents various main interconnections for each set of air chambers. There are 25 possible configurations for rear air suspensions interconnection. For example, chambers 1 can be pitch interconnected while chambers 2 are roll interconnected. Or, it is possible to have one type of interconnection between one set of chambers and the other set is not interconnected (independent).

Table 2- Main interconnection configurations

Main Interconnection Configurations	Active connecting lines ($i=1$)
Independent	$i_r = i_l = i_m = i_b = i_{cr} = i_{cl} = 0$
Pitch Interconnected	$i_r = i_l = 1$
Roll Interconnected	$i_m = i_b = 1$
Cross Interconnected	$i_{cr} = i_{cl} = 1$
All Interconnected	$i_r = i_l = i_m = i_b = i_{cr} = i_{cl} = 1$

4.2.1 Load Distribution

The first and most important goal is to study load distribution between the rear tires. Hence, a new transfer function has been defined, which is the force ratios between the rear tires based on different road excitation inputs. This force ratio is defined as:

$$\begin{aligned}
 & \text{Force Ratio} = FR \\
 FR_{br/mr} &= \frac{F_{gmr}}{F_{gbr}} = \frac{\frac{F_{gmr}}{Z_{gmr}}}{\frac{F_{gbr}}{Z_{gmr}}} \\
 FR_{ml/mr} &= \frac{F_{gmr}}{F_{gml}} = \frac{\frac{F_{gmr}}{Z_{gmr}}}{\frac{F_{gml}}{Z_{gmr}}} \\
 FR_{bl/mr} &= \frac{F_{gmr}}{F_{gbl}} = \frac{\frac{F_{gmr}}{Z_{gmr}}}{\frac{F_{gbl}}{Z_{gmr}}} \quad (4.16)
 \end{aligned}$$

$FR_{br/mr}$, $FR_{ml/mr}$, and $FR_{bl/mr}$ show the force ratio of the second right rear, first left rear, and second left rear tire relative to first right rear tire when the first right rear tire is excited on the road, respectively. The static force has not been considered in this modeling.

Table 3 shows a typical heavy truck specification for the simulations in the next section.

Table 3- Heavy truck specification

Description	Symbol	Value	Unit
Truck sprung mass	M_s	26000	Kg
Truck roll moment of inertia	I_{sx}	50000	$Kg.m^2$
Truck pitch moment of inertia	I_{sy}	150000	$Kg.m^2$
Distance of CG from front axle	L_f	5	m
Distance of CG from first rear axle	L_m	0.5	m
Distance of CG from second rear axle	L_b	2	m
Distance of CG from Right or left suspensions	L_w	0.9	m
Front suspensions equivalent stiffness	K_{sfr}, K_{sfl}	166500	N/m
Rear suspensions equivalent stiffness	K_{smr}, K_{sbr} K_{smb}, K_{sbl}	333000	N/m
Front axle torsional stiffness	K_{tf}	110000	$N.m/rad$
Rear axle torsional stiffness	K_{tr}	110000	$N.m/rad$
Front suspensions damping coefficient	C_{sfr}, C_{sfl}	12500	$N.s/m$
Rear suspensions damping coefficient	C_{smr}, C_{sbr} C_{smb}, C_{sbl}	25000	$N.s/m$
Front tires stiffness	K_{uf}	2500000	N/m
Rear tires stiffness	K_{ur}	5000000	N/m
Front and rear tire damping coefficient	C_{uf}, C_{ur}	0	$N.s/m$

4.3 Main Interconnection Configurations Comparison

The "main interconnection configurations" refers to a situation that both sets of air chambers have the same type of interconnection. For instance, pitch interconnected system means that air

chambers 1 are connected to each other with the same pattern as the air chambers 2 and for both sets, $i_r = i_l = 1$. This analysis reveals the major benefits and drawbacks of the main configurations. Figure 17 to Figure 19 show the Bode diagrams of load distribution between rear tires for main interconnection configurations, when the first right rear tire is excited by the road input.

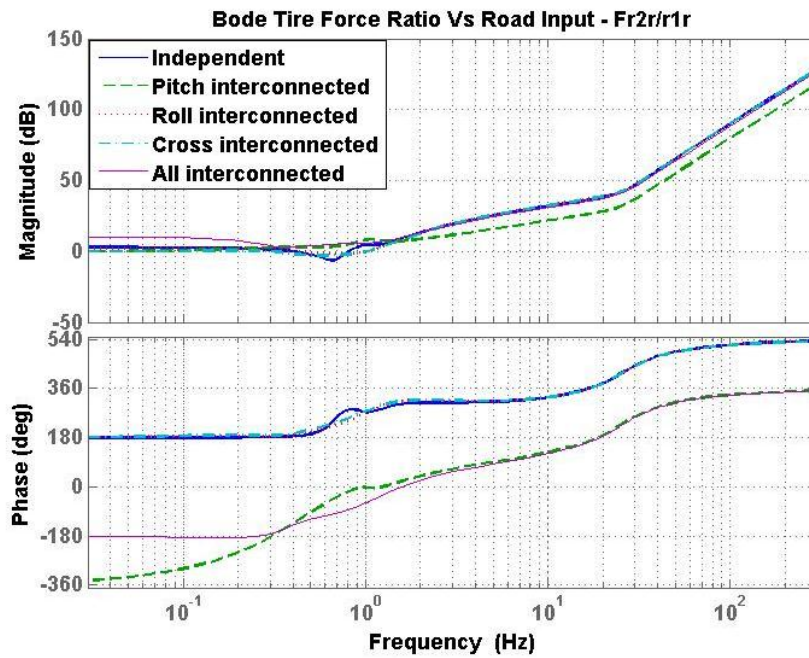


Figure 17- Second right rear tire force ratio respect to first right rear tire

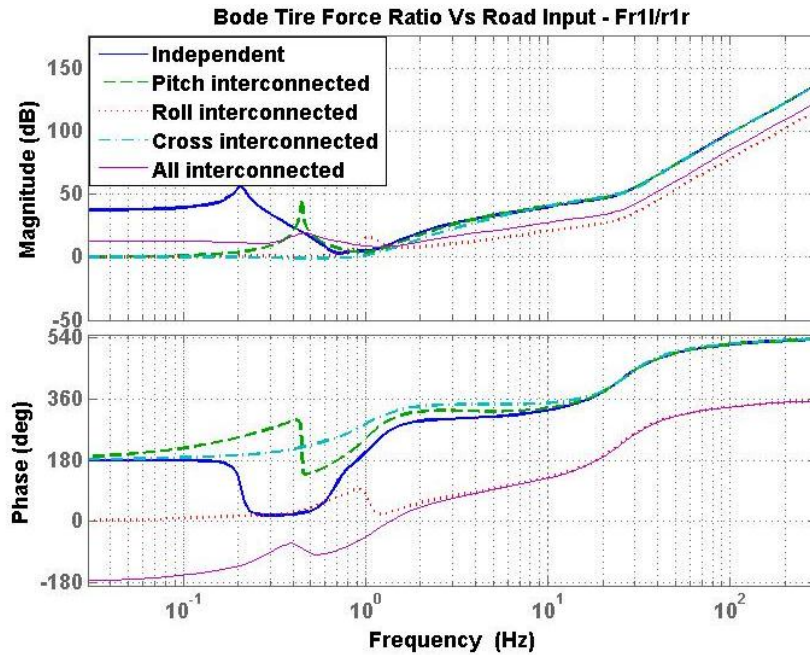


Figure 18- First left rear tire force ratio respect to first right rear tire

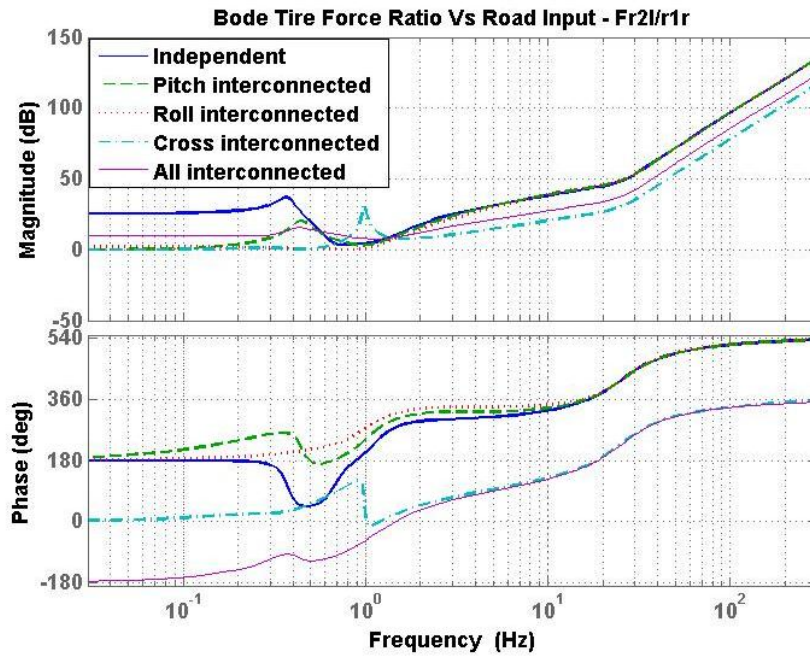


Figure 19- Second left rear tire force ratio respect to first right rear tire

An ideal load distribution configuration means that the force ratio becomes one. It means that the load on the excited tire is transferred to the other tires and force ratio is one (zero decibels). As it can be seen in Figure 17 to Figure 19, the tandem rear tires on each side of the truck take

the advantage of pitch interconnection and the load has been distributed more evenly between them. However, the pitch interconnection does not help system to share the load between the tires on each axle. In other words, pitch interconnection do not improve the load distribution between the right and left tires.

The roll and all interconnected systems work fine in terms of sharing the load between the tires on each axle. On the other hand, just the cross and all connected systems distribute the load between the cross tires. It can be determined that all connected systems do the best job in terms of sharing the load between the right and left side of the truck. However, the configurations that connect the right and left tires to each other (roll, cross, and all interconnected systems) reduce roll stiffness. This drawback will be discussed more in the next sections.

4.3.1 Modal Analysis

The eigenvalues of a system represent the natural frequencies of the system in different modes of motion. To find the eigenvalues, the state space equations of the system are used. "A" matrix shows the inherent characteristics of a system. The eigenvalues are extracted from "A" matrix by solving the following equation:

$$\det(A - \lambda_i I) = 0 \tag{4.17}$$

where λ_i are eigenvalues of the system. The natural frequency and damping ratio of a complex number like " $\lambda_i = a + bj$ " is:

$$\omega_i = |\lambda_i| = \frac{\sqrt{a^2 + b^2}}{2\pi} \text{ (Hz)} \tag{4.18}$$

$$\zeta_i = \frac{|a|}{\sqrt{a^2 + b^2}}$$

Smaller natural frequencies are the dominant modes. Apparently, three main natural frequencies are expected as bounce, pitch, and roll motion frequencies. The natural frequencies for main interconnection configurations are listed in Table 4.

Table 4- System natural frequencies based on the eigenvalues of system

Interconnection Configuration	Bounce (Hz)	Pitch (Hz)	Roll (Hz)
--------------------------------------	--------------------	-------------------	------------------

Without Interconnection	1.2485	1.3448	1.1330
Pitch Interconnected	1.2482	1.2991	1.1330
Roll Interconnected	1.2485	1.3448	0.9304
Cross Interconnected	1.2482	1.2991	0.9304
All Interconnected	1.2482	1.2991	0.9304

As Table 4 shows, the bounce frequency is constant in different configurations, but pitch and roll frequencies are dependent on the type of interconnection. As it was expected, pitch and roll interconnections decrease the pitch and roll frequency. As the cross and all interconnected systems have the characteristics of both pitch and roll interconnected systems, the pitch and roll natural frequencies are decreased. Moreover, the difference between the interconnected and non-interconnected pitch frequency is negligible, but for roll frequency, this difference is about 20%.

4.3.2 Road Simulations

The first step for simulating the suspension system on a road is generating the road profile. For this matter, it is necessary to reconstruct the spectral function into a physical road profile by using ISO 8608, the international standard for road classification. Converting the PSD function representing the specific road profile into a height/distance relationship can be done by [38]:

$$Z_g(x) = \sum_{k=1}^s S_k \sin(2\pi k \Delta\Omega x + \theta_k) \quad (4.19)$$

$$S_k = \sqrt{2(\Delta\Omega)S(k\Delta\Omega)}$$

where, S_k is the amplitude of the excitation harmonics evaluated from PSD function, and $\Delta\Omega$ is the spatial frequency width considered, and θ_k is a random phase angle. Table 5 shows the road roughness for different types of roads.

Table 5- Road classification

Road Class	Roughness Range (mm)	Geometric Mean (mm)
Very good (A)	<8	4
Good (B)	8-32	16
Average (C)	32-128	64

Poor (D)	128-512	256
Very poor (E)	512-2048	1024

Figure 20 shows different road profiles with the same phase but with a different magnitude of roughness.

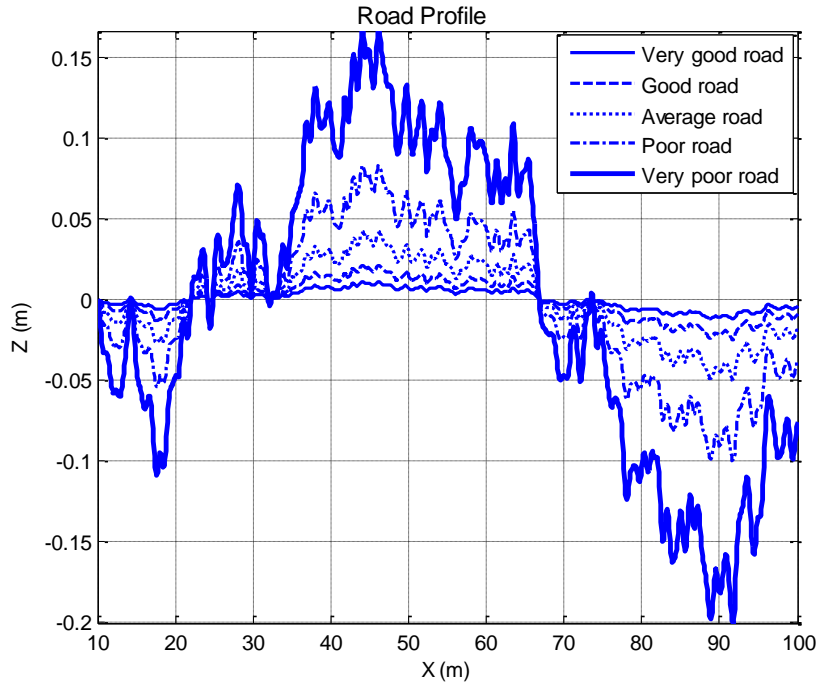


Figure 20- Different types of the roads

In this thesis, poor road (D) has been chosen for the simulation of the interconnected suspension in a harsh situation. By running the Matlab code (Appendix 2) the tire force and motion of the vehicle body can be calculated based on the generated road profile. To compare the tire load in different interconnection configurations, the root mean square (RMS) and the maximum tire force are used.

Table 6- RMS rear tire force (e4) with different main interconnection configurations

Main Configurations	First right rear tire force (mr)		First right rear tire force (mr)		Second right rear tire force (br)		Second left rear tire force (bl)		All tires average
Independent	2.090	100%	2.132	100%	2.013	100%	2.043	100%	100%
Pitch Int.	2.053	98.2%	2.097	98.3%	2.051	101.9%	2.080	101.8%	100%

Roll Int.	1.807	86.5%	1.847	86.6%	1.781	88.5%	1.811	88.6%	87%
Cross Int.	1.820	87.1%	1.857	87.1%	1.772	88.1%	1.798	88%	87.6%
All Int.	1.802	86.2%	1.841	86.3%	1.789	88.9%	1.816	88.9%	87.6%

Table 7- Maximum rear tires force (e4) with different main interconnection configurations

Main Configurations	First right rear tire force (mr)		First right rear tire force (mr)		Second right rear tire force (br)		Second left rear tire force (bl)		All tires average
	Force (kN)	Percentage (%)	Force (kN)	Percentage (%)	Force (kN)	Percentage (%)	Force (kN)	Percentage (%)	
Independent	7.002	100%	5.969	100%	6.483	100%	5.437	100%	100%
Pitch Int.	7.070	101%	5.900	98.8%	6.624	102%	5.653	104%	101.5%
Roll Int.	5.906	84.3%	5.406	90.6%	5.627	86.8%	5.497	101%	90.7%
Cross Int.	5.953	85%	5.690	95.3%	5.683	87.6%	5.29	97.4%	91.3%
All Int.	5.924	84.6%	5.396	90.4%	5.677	87.5%	5.498	101%	90.9%

Table 6 and Table 7 show the RMS and maximum rear tire forces over one kilometer poor road at the speed of 10 (m/s), respectively. As it can be seen in the tables, roll, cross, and all interconnected systems improve the load distribution by about 10% compared with the conventional independent air suspension system (non-interconnected). But the pitch interconnection does not help to distribute the load more evenly between tires.

Interconnection of air suspensions does not have significant impact on the bounce, pitch, and roll motion of body. As Table 8 represents, different kinds of interconnections do not have any effect on the bounce motion and just the cross interconnection can improve the performance of suspension for both roll and pitch motion.

Table 8- Bounce, pitch, and roll motion of body

Main Configurations	Bounce (m)		Pitch angle (deg)		Roll angle (deg)	
	Force (kN)	Percentage (%)	Force (kN)	Percentage (%)	Force (kN)	Percentage (%)
Independent	0.0327	100%	0.2229	100%	2.2256	100%
Pitch Int.	0.0327	100%	0.2098	94%	2.2256	100%
Roll Int.	0.0327	100%	0.2229	100%	2.1313	95.7%
Cross Int.	0.0327	100%	0.2098	94%	2.1313	95.7%
All Int.	0.0327	100%	0.2098	94%	2.1313	95.7%

4.4 Interconnection Configurations Comparison

After studying the main interconnection configurations (when both sets of air chambers are connected with the same pattern), it is time to research for the other configurations which have different type of interconnections for air chambers 1 and 2. The first question is about the effect of each set of chambers on the total performance of the suspension system. To investigate on this matter, modal analysis will be used. As it has been discussed, interconnection does not change the bounce stiffness of vehicle. Also, pitch interconnection has only influence on pitch natural frequency and roll interconnection does the same, on the roll natural frequency of vehicle. Moreover, cross and all interconnection configurations have impact on both roll and pitch stiffness.

Table 9- Different configurations for roll interconnection

Air chamber 1s interconnection configuration	Air chamber 2s interconnection configuration	Roll natural frequency (Hz)	
Independent	Independent	1.1330	100%
Roll Int.	Independent	1.0788	91%
Independent	Roll Int.	0.9985	78%
Roll Int.	Roll Int.	0.9304	67%

Table 10- Different configurations for pitch interconnection

Air chamber 1s interconnection configuration	Air chamber 2s interconnection configuration	Pitch natural frequency (Hz)	
Independent	Independent	1.3448	100%
Pitch Int.	Independent	1.3319	98%
Independent	Pitch Int.	1.3136	95%
Pitch Int.	Pitch Int.	1.2991	93%

Table 11- Different configurations for cross and all interconnection

Air chamber 1s interconnection configuration	Air chamber 2s interconnection configuration	Pitch natural frequency (Hz)		Roll natural frequency (Hz)	
		Frequency (Hz)	Percentage	Frequency (Hz)	Percentage
Independent	Independent	1.3448	100%	1.1330	100%
Cross or all Int.	Independent	1.3319	98%	1.0788	91%
Independent	Cross or all Int.	1.3136	95%	0.9985	78%
Cross or all Int.	Cross or all Int.	1.2991	93%	0.9304	67%

As Table 9 represents, roll stiffness is decreased step by step after connecting the air chambers with roll configuration. Roll interconnection of air chambers 1, (smaller chambers) decreases the roll natural frequency by 9% and roll interconnection of air chambers 2 decreases the roll natural frequency by 22%. Finally, interconnection of both sets reduces the roll natural frequency by 23%. Table 10 shows similar results for the pitch interconnection and pitch natural frequency. In the full pitch interconnection mode (when both sets of air chambers are pitch interconnected) the frequency drops by 7%.

Based on Table 11, cross and all interconnection configurations have same natural frequencies. In terms of roll and pitch natural frequencies, they behave exactly same as the roll and pitch interconnection modes, respectively.

4.5 Lower Order Model Analysis

In order to have a better understanding about the suspension system, a simplified model is preferred. To do so, the unsprung mass and unsprung spring are removed. Removing each unsprung mass removes two states of the system, and consequently, the order of the system would be lowered. However, before doing this simplification, it is necessary to study the changes in the system outputs by removing the unsprung masses. Hence, a quarter car model shown in Figure 21 is used. The unsprung mass includes the tire's mass and joints; unsprung stiffness is related to the tire's properties. The damping coefficient of the tire is assumed to be zero.

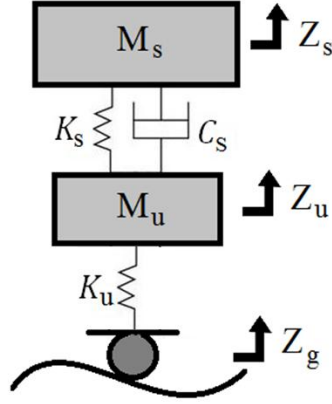


Figure 21- Quarter car model with unsprung mass

Using the model in Figure 21, the state space of the system can be extracted as:

$$\begin{aligned}
 \begin{bmatrix} \ddot{Z}_s \\ \ddot{Z}_u \\ \dot{Z}_s \\ \dot{Z}_u \\ \dot{x} \end{bmatrix} &= \underbrace{\begin{bmatrix} -\frac{C_s}{M_s} & \frac{C_s}{M_s} & -\frac{K_s}{M_s} & \frac{K_s}{M_s} \\ \frac{C_s}{m_u} & -\frac{C_s}{m_u} & \frac{K_s}{m_u} & -\frac{K_s + K_u}{m_u} \\ 1 & 0 & 0 & 0 \\ 0 & 1 & 0 & 0 \end{bmatrix}}_A \begin{bmatrix} \dot{Z}_s \\ \dot{Z}_u \\ Z_s \\ Z_u \end{bmatrix} + \underbrace{\begin{bmatrix} 0 \\ \frac{K_u}{m_u} \\ 0 \\ 0 \end{bmatrix}}_B \begin{bmatrix} Z_g \\ U \end{bmatrix} \\
 Y = [F_{tire}] &= \underbrace{\begin{bmatrix} 0 & 0 & 0 & -K_u \end{bmatrix}}_{C^T} \underbrace{\begin{bmatrix} \dot{Z}_s \\ \dot{Z}_u \\ Z_s \\ Z_u \end{bmatrix}}_X + \underbrace{\begin{bmatrix} K_u \end{bmatrix}}_D \underbrace{\begin{bmatrix} Z_g \\ U \end{bmatrix}}_U
 \end{aligned} \tag{4.20}$$

where, Z_g is the road input (road profile), Z_s is the sprung mass displacement, and Z_u is the unsprung mass displacement. The output is the tire force defined based on the tire deflection.

The transfer function of the tire force (output) relative to road profile (input) is:

$$\frac{F_{tire}}{Z_g} = \frac{K_u M_s m_u s^4 + K_u C_s (M_s + m_u) s^3 + K_u K_s (M_s + m_u) s^2}{M_s m_u s^4 + C_s (M_s + m_u) s^3 + (K_s (M_s + m_u) + K_u M_s) s^2 + K_u C_s s + K_u K_s} \tag{4.21}$$

In most vehicles, sprung mass is approximately 10 times heavier than the unsprung mass and tire stiffness is 10 times more than the suspension stiffness. Therefore, the transfer function is simplified to:

$$\begin{cases} m_u = \frac{M_s}{20} \\ K_u = 10 K_s \end{cases} \Rightarrow \frac{F_{tire}}{Z_g} = \frac{10K_s M_s^2 s^4 + 210K_s M_s C_s s^3 + 210K_s^2 M_s s^2}{M_s^2 s^4 + 21C_s M_s s^3 + 221K_s M_s s^2 + 200K_s C_s s + 200K_s^2} \quad (4.22)$$

For the next step, a quarter car model without unsprung mass shown in Figure 22 is proposed to see the differences between this model and previous model (with sprung mass).

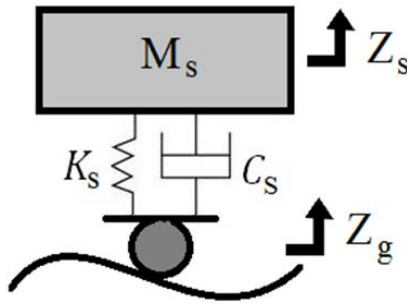


Figure 22- Quarter car model without unsprung mass

Using Figure 22, the state space equations are:

$$\begin{aligned} \begin{bmatrix} \ddot{Z}_s \\ \dot{Z}_s \\ \dot{Z}_s \end{bmatrix} &= \underbrace{\begin{bmatrix} -\frac{C_s}{M_s} & -\frac{K_s}{M_s} \\ 1 & 0 \end{bmatrix}}_A \begin{bmatrix} \dot{Z}_s \\ Z_s \end{bmatrix} + \underbrace{\begin{bmatrix} \frac{C_s}{M_s} & \frac{K_s}{M_s} \\ 0 & 0 \end{bmatrix}}_B \begin{bmatrix} \dot{Z}_g \\ Z_g \end{bmatrix} \\ Y = [F_{tire}] &= \underbrace{[-C_s \quad -K_s]}_{C^T} \begin{bmatrix} \dot{Z}_s \\ Z_s \end{bmatrix} + \underbrace{[C_s \quad K_s]}_{D} \begin{bmatrix} \dot{Z}_g \\ Z_g \end{bmatrix} \end{aligned} \quad (4.23)$$

Because the damper is in touch with the road, the derivative of road profile has to be counted in. Considering the relation between the inputs ($\dot{Z}_g = s Z_g$), the transfer functions can be merged.

$$\frac{F_{tire}}{\dot{Z}_g} = \frac{M_s C_s s^2}{M_s s^2 + C_s s + K_s} \quad \frac{F_{tire}}{Z_g} = \frac{M_s K_s s^2}{M_s s^2 + C_s s + K_s} \quad (4.24)$$

$$\dot{Z}_g = s Z_g \Rightarrow \frac{F_{tire}}{\text{Road Excitation}} = \frac{F_{tire}}{Z_g} + s \frac{F_{tire}}{\dot{Z}_g} = \frac{M_s C_s s^3 + M_s K_s s^2}{M_s s^2 + C_s s + K_s}$$

To compare the transfer functions which are obtained from the different models (with and without unsprung mass), Bode diagram in frequency domain is used.

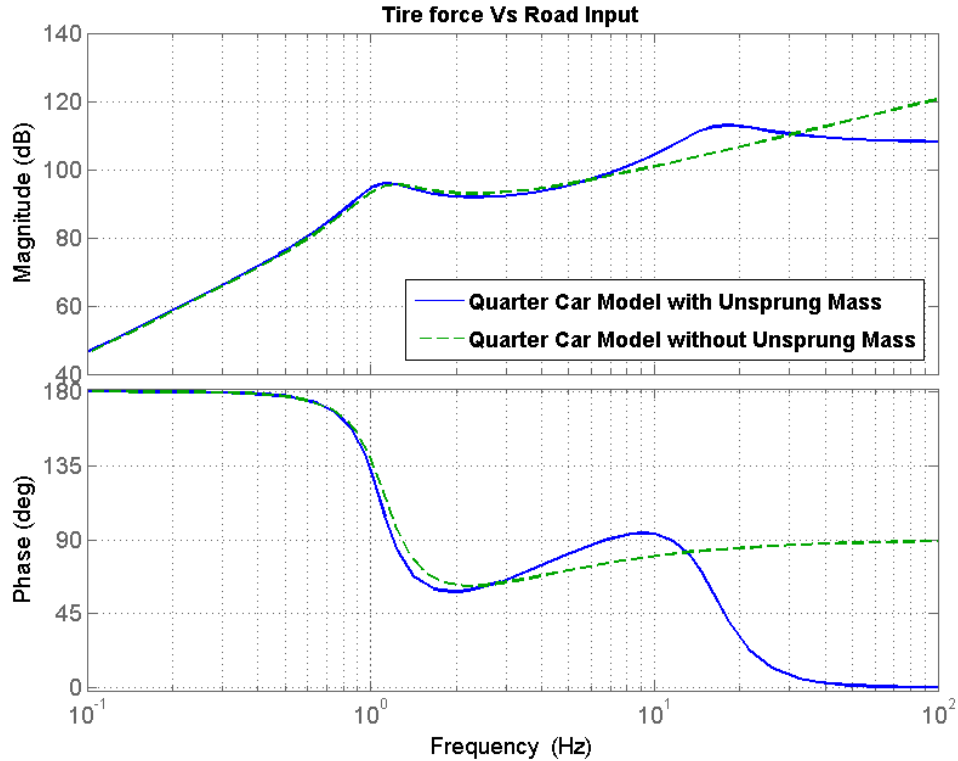


Figure 23- Bode plot of quarter car models

As Figure 23 shows, both models are perfectly matched in low frequencies - less than 10 hertz. This range of frequency is enough for the studies on the suspension and load distribution studies.

By comparing the analytical format of transfer functions, same result can be obtained. The higher order terms have more effect in high frequencies, and the lower order terms in the numerator and denominator play an essential role in low frequencies. The first two low-order terms in both transfer functions are:

$$\begin{aligned}
 \left(\frac{F_{tire}}{Z_g} \right)_{\text{with Unsprung}} &\xrightarrow{\text{Low Frequencies}} \frac{210K_s M_s C_s s^3 + 210K_s^2 M_s s^2}{200K_s C_s s + 200K_s^2} = 1.05 \left(s^2 \frac{M_s C_s s + K_s M_s}{C_s s + K_s} \right) = 1.05 M_s s^2 \\
 \left(\frac{F_{tire}}{Z_g} \right)_{\text{without Unsprung}} &\xrightarrow{\text{Low Frequencies}} s^2 \frac{M_s C_s s + M_s K_s}{C_s s + K_s} = M_s s^2
 \end{aligned}
 \tag{4.25}$$

It is clear that at low frequencies, both transfer functions have similar behavior.

4.5.1 Truck Pitch Model

To simplify the model further, a half car model without unsprung mass is used in order to analyze the pitch motion without being concerned about the roll motion.

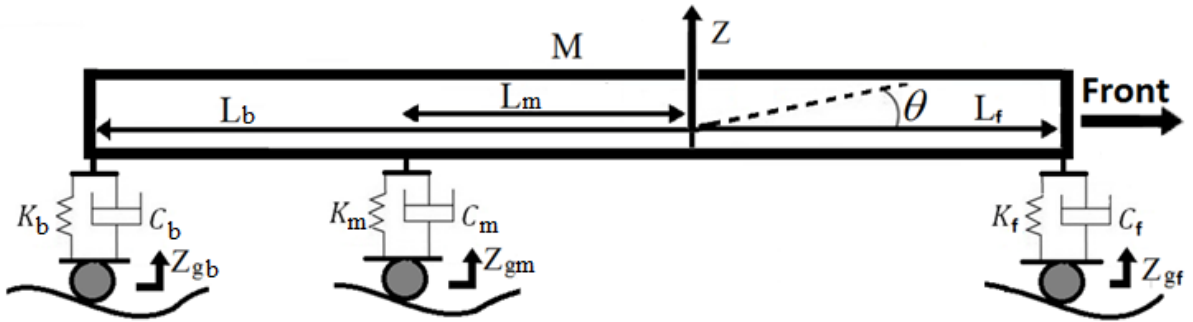


Figure 24- Half car model for three axle truck

Figure 24 shows the truck half model with three axles that has bounce (Z) and pitch (θ) motion. The dynamic equations in the state space format are:

$$\begin{aligned}
\begin{bmatrix} \ddot{Z} \\ \ddot{\theta} \\ \dot{Z} \\ \dot{\theta} \end{bmatrix} &= \underbrace{\begin{bmatrix} A_{C_min\ 2 \times 2} & \dots & A_{K_min\ 2 \times 2} \\ 1 & 0 & 0 & 0 \\ 0 & 1 & 0 & 0 \end{bmatrix}}_{A_{4 \times 4}} \begin{bmatrix} \dot{Z} \\ \dot{\theta} \\ Z \\ \theta \end{bmatrix} + \underbrace{\begin{bmatrix} B_{min\ 2 \times 6} \\ 0_{2 \times 6} \end{bmatrix}}_{B_{4 \times 6}} \begin{bmatrix} \dot{Z}_{gf} \\ \dot{Z}_{gm} \\ \dot{Z}_{gb} \\ Z_{gf} \\ Z_{gm} \\ Z_{gb} \end{bmatrix} \\
Y = \begin{bmatrix} F_{gf} \\ F_{gm} \\ F_{gb} \end{bmatrix} &= \underbrace{\begin{bmatrix} -C_f & -L_f C_f & -K_f & -L_f K_f \\ -C_m & L_m C_m & -K_m & L_m K_m \\ -C_b & L_b C_b & -K_b & L_b K_b \end{bmatrix}}_{C_{3 \times 4}} \begin{bmatrix} \dot{Z} \\ \dot{\theta} \\ Z \\ \theta \end{bmatrix} + \underbrace{\begin{bmatrix} C_f & 0 & 0 & K_f & 0 & 0 \\ 0 & C_m & 0 & 0 & K_m & 0 \\ 0 & 0 & C_b & 0 & 0 & K_b \end{bmatrix}}_{D_{3 \times 6}} \begin{bmatrix} \dot{Z}_{gf} \\ \dot{Z}_{gm} \\ \dot{Z}_{gb} \\ Z_{gf} \\ Z_{gm} \\ Z_{gb} \end{bmatrix}
\end{aligned} \tag{4.26}$$

$$\begin{aligned}
[A_{C_min\ 2 \times 2}] &= \begin{bmatrix} -\frac{C_f + C_m + C_b}{M} & \frac{-L_f C_f + L_m C_m + L_b C_b}{M} \\ -\frac{L_f C_f + L_m C_m + L_b C_b}{I_y} & -\frac{L_f^2 C_f + L_m^2 C_m + L_b^2 C_b}{I_y} \end{bmatrix} \\
[A_{K_min\ 2 \times 2}] &= \begin{bmatrix} -\frac{K_f + K_m + K_b}{M} & \frac{-L_f K_f + L_m K_m + L_b K_b}{M} \\ -\frac{L_f K_f + L_m K_m + L_b K_b}{I_y} & -\frac{L_f^2 K_f + L_m^2 K_m + L_b^2 K_b}{I_y} \end{bmatrix} \\
[B_{min\ 2 \times 4}] &= \begin{bmatrix} \frac{C_f}{M} & \frac{C_m}{M} & \frac{C_b}{M} & \frac{K_f}{M} & \frac{K_m}{M} & \frac{K_b}{M} \\ \frac{L_f C_f}{I_y} & \frac{L_m C_m}{I_y} & \frac{L_b C_b}{I_y} & \frac{L_f K_f}{I_y} & \frac{L_m K_m}{I_y} & \frac{L_b K_b}{I_y} \end{bmatrix}
\end{aligned} \tag{4.27}$$

Like the previous models, the outputs of the system are the tire forces (F_g), and the inputs are the road profiles and their derivatives (Z_g).

For the pitch interconnected system, the overall definition of state space and damping sub-matrixes are the same. The following are the model matrices for the pitch interconnected half truck model:

$$\begin{aligned}
& K_m = K_b = K_r \\
& \left[A_{K_min}^{2 \times 2} \right]_{Pitch-Int} = \begin{bmatrix} -\frac{K_f + 2K_r}{M} & \frac{-L_f K_f + (L_m + L_b)K_r}{M} \\ \frac{-L_f K_f + (L_m + L_b)K_r}{I_y} & \frac{L_f^2 K_f + K_r \frac{(L_m + L_b)^2}{2}}{I_y} \end{bmatrix} \\
& \left[B_{min}^{2 \times 6} \right]_{Pitch-Int} = \begin{bmatrix} \frac{C_f}{M} & \frac{C_m}{M} & \frac{C_b}{M} & \frac{K_f}{M} & \frac{K_r}{M} & \frac{K_r}{M} \\ \frac{L_f C_f}{I_y} & -\frac{L_m C_m}{I_y} & -\frac{L_b C_b}{I_y} & \frac{L_f K_f}{I_y} & -\frac{(L_m + L_b)K_r}{2I_y} & -\frac{(L_m + L_b)K_r}{2I_y} \end{bmatrix} \\
& \left[C_{3 \times 4} \right]_{Pitch-Int} = \begin{bmatrix} -C_f & -L_f C_f & -K_f & -L_f K_f \\ -C_m & L_m C_m & -K_r & \frac{(L_m + L_b)K_r}{2} \\ -C_b & L_b C_b & -K_r & \frac{(L_m + L_b)K_r}{2} \end{bmatrix} \quad \left[D_{3 \times 6} \right]_{Pitch-Int} = \begin{bmatrix} C_f & 0 & 0 & K_f & 0 & 0 \\ 0 & C_m & 0 & 0 & \frac{K_r}{2} & \frac{K_r}{2} \\ 0 & 0 & C_b & 0 & \frac{K_r}{2} & \frac{K_r}{2} \end{bmatrix} \quad (4.28)
\end{aligned}$$

Another simplifying fact about the truck model is that the rear axle suspensions are the same and they have the same stiffness and damping ratio. Normally, the front suspension has a spring and damper with half capacity because the load on the front tire is about half of rear ones. In the model, it is assumed that the front suspension stiffness and damping coefficient is approximately half of the rear ones. α factor is defined for the front suspension elements which is approximately 0.5. The simplifying assumptions result in:

$$\begin{aligned}
K_m = K_b = K & & C_m = C_b = C \\
K_f = \alpha K & & C_f = \alpha C
\end{aligned} \quad (4.29)$$

After solving the state space equations to find the transfer functions, there are 18 different transfer functions relating the output (3 tire forces) to the 6 inputs (road inputs). Considering the relation between the inputs ($\dot{Z}_g = s Z_g$), the transfer functions can be merged to:

$$\frac{F_{tire}}{Road\ Excitation} = \frac{F_g}{RE} \quad (4.30)$$

$$\left\{ \begin{array}{l} \frac{F_{gm}}{RE_m} = s \frac{F_{gm}}{\dot{Z}_{gm}} + \frac{F_{gm}}{Z_{gm}} \\ \frac{F_{gb}}{RE_m} = s \frac{F_{gb}}{\dot{Z}_{gm}} + \frac{F_{gb}}{Z_{gm}} \end{array} \right. \quad \left\{ \begin{array}{l} \frac{F_{gm}}{RE_b} = s \frac{F_{gm}}{\dot{Z}_{gb}} + \frac{F_{gm}}{Z_{gb}} \\ \frac{F_{gb}}{RE_b} = s \frac{F_{gb}}{\dot{Z}_{gb}} + \frac{F_{gb}}{Z_{gb}} \end{array} \right.$$

To investigate the load distribution between the rear tires, new transfer functions are defined. Transfer functions are force ratios between rear tires based on the different road excitation inputs as:

$$\begin{aligned} & \text{Force Ratio} = FR \\ FR_m &= \frac{\frac{F_{gm}}{RE_m}}{\frac{F_{gb}}{RE_m}} = \frac{s \frac{F_{gm}}{\dot{Z}_{gm}} + \frac{F_{gm}}{Z_{gm}}}{s \frac{F_{gb}}{\dot{Z}_{gm}} + \frac{F_{gb}}{Z_{gm}}} \quad (4.31) \end{aligned}$$

FR_m shows the force ratio of the first rear tire relative to the second rear tire when the first rear tire is excited by the road. The static force of tires due to the weight of sprung mass is not considered. Transfer functions for independent and interconnected air suspensions are:

$$FR_{rm} = \frac{a_4 s^4 + a_3 s^3 + a_2 s^2 + a_1 s + a_0}{b_3 s^3 + b_2 s^2 + b_1 s + b_0}$$

$$\begin{aligned} a_4 &= I_y M & b_3 &= C(I_y + ML_m L_b) \\ a_3 &= I_y C(\alpha + 1) + MC(L_f^2 \alpha + L_b^2) & b_2 &= \frac{K}{C} b_3 + \alpha C^2 (L_f + L_b)(L_f + L_m) \\ a_2 &= \frac{K}{C} a_3 + \alpha C^2 (L_f + L_b)^2 & b_1 &= 2\alpha CK(L_f + L_b)(L_f + L_m) \\ a_1 &= 2\alpha CK(L_f + L_b)^2 & b_0 &= \alpha K^2 (L_f + L_b)(L_f + L_m) \\ a_0 &= \alpha K^2 (L_f + L_b)^2 \end{aligned}$$

$$FR_{rm_Pitch_Int} = \frac{a_4 s^4 + a_3 s^3 + a_2 s^2 + a_1 s + a_0}{b_3 s^3 + b_2 s^2 + b_1 s + b_0}$$

$$\begin{aligned} a_4 &= 2CI_y M & b_3 &= 2C^2(I_y + ML_m L_b) - KMI_y \\ a_3 &= 2C^2(I_y(\alpha + 1) + M(L_f^2 \alpha + L_b^2)) + KMI_y & b_2 &= \frac{C^2}{K^2} b_0 + CK(\alpha(I_y + L_f^2 M) + 2(I_y + L_m L_b M)) \\ a_2 &= \frac{C^2}{K^2} a_0 + CK(3\alpha(I_y + L_f^2 M) + 2(I_y + L_b^2 M)) & b_1 &= 2\frac{C}{K} b_0 - \alpha K^2(I_y + L_f^2 M) \\ a_1 &= 2\frac{C}{K} a_0 + \alpha K^2(I_y + L_f^2 M) & b_0 &= 2\alpha CK^2(L_f + L_b)(L_f + L_m) \\ a_0 &= 2\alpha CK^2(L_f + L_b)^2 \end{aligned}$$

(4.32)

As shown in the transfer functions, coefficients of higher order terms are mostly a function of the damping coefficient, and coefficients of lower order terms are functions of stiffness. This is because the spring plays an essential role in low frequencies, and damper has an important impact on the suspension performance in high frequencies where the speed of excitation is high. In other words, the interconnection improves the suspension performance in low speeds. Since, an interconnection does not change the damping characteristics, the behavior of the suspension system will remain the same in high speeds.

The Bode plot for a typical heavy truck with the specification listed in Table 12 is shown in Figure 25.

Table 12- Heavy truck specification for pitch model

Description	Symbol	Value	Unit
Half truck sprung mass	M	13000	Kg

Half truck moment of inertia	I_y	75000	$Kg.m^2$
Front Suspension coefficient	α	0.5	-
Rear Suspensions stiffness	K	333000	N/m
Rear suspensions damping coefficient	C	25000	$N.s/m$
Distance of CG from front axle	L_F	5	M
Distance of CG from first rear axle	L_m	0.5	M
Distance of CG from second rear axle	L_b	2	M

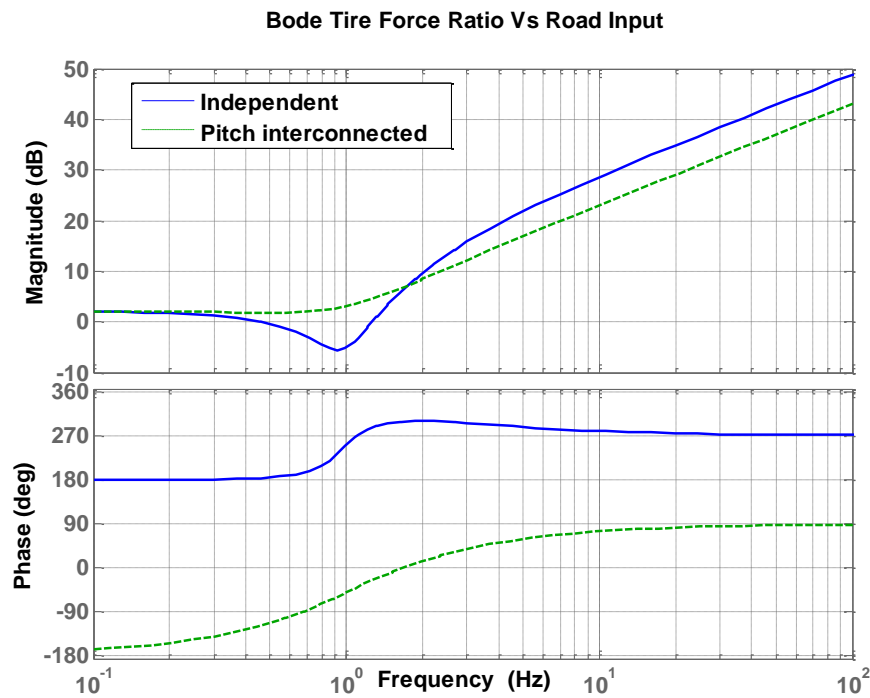


Figure 25- Rear tires force ratio

As Figure 25 represents, the pitch interconnected system has better performance in terms of load distribution. This means that the rear suspensions distribute load more evenly. In high frequencies, the force ratio of the pitch interconnected system is half of the independent system, and operates two times better than independent system. In low frequencies especially around 1 Hertz, the force ratio of the pitch interconnected suspension is closer to one.

Another issue that should be investigated is the vehicle pitch stiffness which is defined based on the angular pitch displacement of the sprung body ($\Delta\theta$) against the applied torque on the body. This can be shown as:

$$\begin{aligned} \tau - (K_f L_f \Delta\theta) L_f - (K_m L_m \Delta\theta) L_m - (K_b L_b \Delta\theta) L_b &= 0 \\ K_{Tor} = \frac{\tau}{\Delta\theta} &= K_f L_f^2 + K_m L_m^2 + K_b L_b^2 \end{aligned} \quad (4.33)$$

For a simplified pitch interconnected model, pitch stiffness is:

$$\begin{aligned} \tau - (K_f L_f \Delta\theta) L_f - \left(K_r \left(\frac{L_m \Delta\theta + L_b \Delta\theta}{2} \right) \right) (L_m + L_b) &= 0 \\ K_{Tor_Pitch_Int} = \frac{\tau}{\Delta\theta} &= K_f L_f^2 + \frac{1}{2} K_r (L_m + L_b)^2 \end{aligned} \quad (4.34)$$

The stiffness of front springs is approximately half of the rear ones. Therefore, the pitch stiffness of the interconnected system in comparison with the independent suspension system is:

$$\frac{K_{Tor_Pitch_Int}}{K_{Tor}} \stackrel{\substack{K_m=K_b=K \\ K_f=\alpha K}}{=} \frac{K \left(\alpha L_f^2 + L_m^2 + L_b^2 \right)}{K \left(\alpha L_f^2 + \frac{(L_m + L_b)^2}{2} \right)} \approx 93\% \quad (4.35)$$

For a typical heavy truck (Table 12), the pitch stiffness of the interconnected system is 93% of a normal suspension system without interconnection. It means that pitch interconnection decreases the pitch stiffness by 7% and the effect of this reduction on the system behavior is negligible.

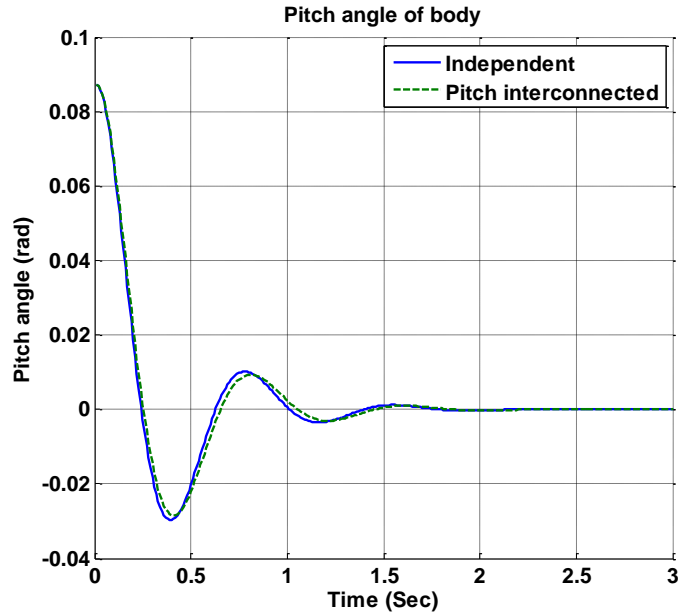


Figure 26- Pitch motion of sprung body

Figure 26 represents the time response of the sprung body when 5 degrees (0.087 rad) initial pitch angle is applied to the body. As shown, the pitch interconnected system settles down slower because of lower pitch stiffness. However, the difference between the two models is negligible.

4.5.2 Truck Roll Model

In order to study the roll motion (ϕ) of the body, the focus will be on the right and left suspensions. Figure 27 shows the truck front view.

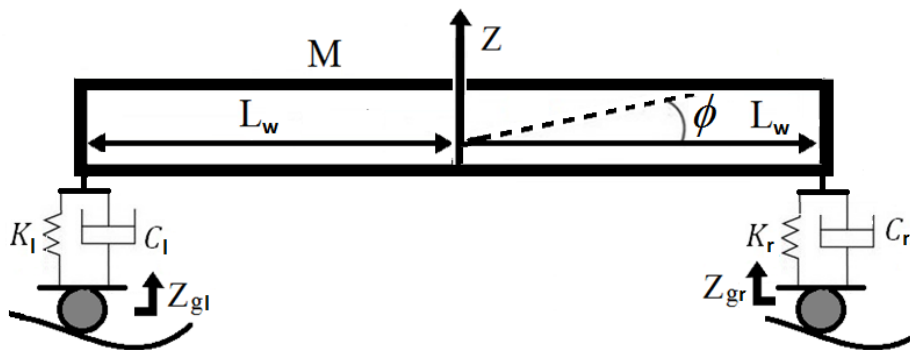


Figure 27- Front view of truck

The state space equations are:

$$\begin{bmatrix} \ddot{Z} \\ \ddot{\phi} \\ \dot{Z} \\ \dot{\phi} \end{bmatrix} = \underbrace{\begin{bmatrix} A_{C_min\ 2 \times 2} & A_{K_min\ 2 \times 2} \\ 1 & 0 & 0 & 0 \\ 0 & 1 & 0 & 0 \end{bmatrix}}_{A_{4 \times 4}} \begin{bmatrix} \dot{Z} \\ \dot{\phi} \\ Z \\ \phi \end{bmatrix} + \underbrace{\begin{bmatrix} B_{min\ 2 \times 4} \\ 0_{2 \times 4} \end{bmatrix}}_{B_{4 \times 4}} \begin{bmatrix} \dot{Z}_{gr} \\ \dot{Z}_{gl} \\ Z_{gr} \\ Z_{gl} \end{bmatrix} \quad (4.36)$$

$$Y = \begin{bmatrix} F_{gr} \\ F_{gl} \end{bmatrix} = \underbrace{\begin{bmatrix} -C_r & -L_w C_r & -K_r & -L_w K_r \\ -C_l & L_w C_l & -K_l & L_w K_l \end{bmatrix}}_C \begin{bmatrix} \dot{\phi} \\ Z \\ \phi \end{bmatrix} + \underbrace{\begin{bmatrix} C_r & 0 & K_r & 0 \\ 0 & C_l & 0 & K_l \end{bmatrix}}_D \begin{bmatrix} \dot{Z}_{gr} \\ \dot{Z}_{gl} \\ Z_{gr} \\ Z_{gl} \end{bmatrix}$$

$$\begin{aligned} [A_{C_min\ 2 \times 2}] &= \begin{bmatrix} -\frac{C_r + C_l}{M} & -\frac{L_w(C_r - C_l)}{M} \\ -\frac{L_w(C_r - C_l)}{I_y} & -\frac{L_w^2(C_r + C_l)}{I_y} \end{bmatrix} \\ [A_{K_min\ 2 \times 2}] &= \begin{bmatrix} -\frac{K_r + K_l}{M} & -\frac{L_w(K_r - K_l)}{M} \\ -\frac{L_w(K_r - K_l)}{I_y} & -\frac{L_w^2(K_r + K_l)}{I_y} \end{bmatrix} \\ [B_{min\ 2 \times 4}] &= \begin{bmatrix} \frac{C_r}{M} & \frac{C_l}{M} & \frac{K_r}{M} & \frac{K_l}{M} \\ \frac{L_w C_r}{I_y} & -\frac{L_w C_l}{I_y} & \frac{L_w K_r}{I_y} & -\frac{L_w K_l}{I_y} \end{bmatrix} \end{aligned} \quad (4.37)$$

Like the previous models, the outputs of the system are tires forces (F_g), and the inputs are road profiles and their derivatives (Z_g).

For roll interconnected system, new sub matrixes are:

$$\begin{aligned} K_r &= K_l = K \\ [A_{K_min\ 2 \times 2}^{Roll-Int}] &= \begin{bmatrix} -\frac{2K}{M} & 0 \\ 0 & 0 \end{bmatrix} & [B_{min\ 2 \times 4}^{Roll-Int}] &= \begin{bmatrix} \frac{C_r}{M} & \frac{C_l}{M} & \frac{K}{M} & \frac{K}{M} \\ \frac{L_w C_r}{I_y} & -\frac{L_w C_l}{I_y} & 0 & 0 \end{bmatrix} \\ [C_{2 \times 4}^{Roll-Int}] &= \begin{bmatrix} -C_r & -L_w C_r & -K & 0 \\ -C_l & L_w C_l & -K & 0 \end{bmatrix} & [D_{2 \times 4}^{Roll-Int}] &= \begin{bmatrix} C_r & 0 & \frac{K}{2} & \frac{K}{2} \\ 0 & C_l & \frac{K}{2} & \frac{K}{2} \end{bmatrix} \end{aligned} \quad (4.38)$$

By considering this fact that right and left suspension components are the same ($K_r = K_l = K$ and $C_r = C_l = C$), the force ratio transfer functions for independent and roll interconnected suspension systems respectively will be:

$$FR_r = \frac{\frac{F_{gr}}{RE_r}}{\frac{F_{gl}}{RE_r}} = \frac{s \frac{F_{gr}}{Z_{gr}} + \frac{F_{gr}}{Z_{gr}}}{s \frac{F_{gl}}{Z_{gr}} + \frac{F_{gl}}{Z_{gr}}} = \frac{MI_x s^2 + C(I_x + L_w^2 M)s + K(I_x + L_w^2 M)}{C(I_x - L_w^2 M)s + K(I_x - L_w^2 M)} \quad (4.39)$$

$$FR_{r_Roll_Int} = \frac{MI_x s^2 + C(I_x + L_w^2 M)s + K(I_x + \frac{M}{C})}{C(I_x - L_w^2 M)s + K(I_x - \frac{M}{C})}$$

The Bode plot for a typical heavy truck with a specification listed in Table 13 is:

Table 13- Heavy truck specification for roll model

Description	Symbol	Value	Unit
Half truck sprung mass	M	10400	Kg
Half truck moment of inertia	I_x	20000	$Kg.m^2$
Right or left Suspensions stiffness	K	333000	N/m
Right or left suspensions damping coefficient	C	25000	$N.s/m$
Distance of CG from Right or left suspensions	L_w	0.9	m

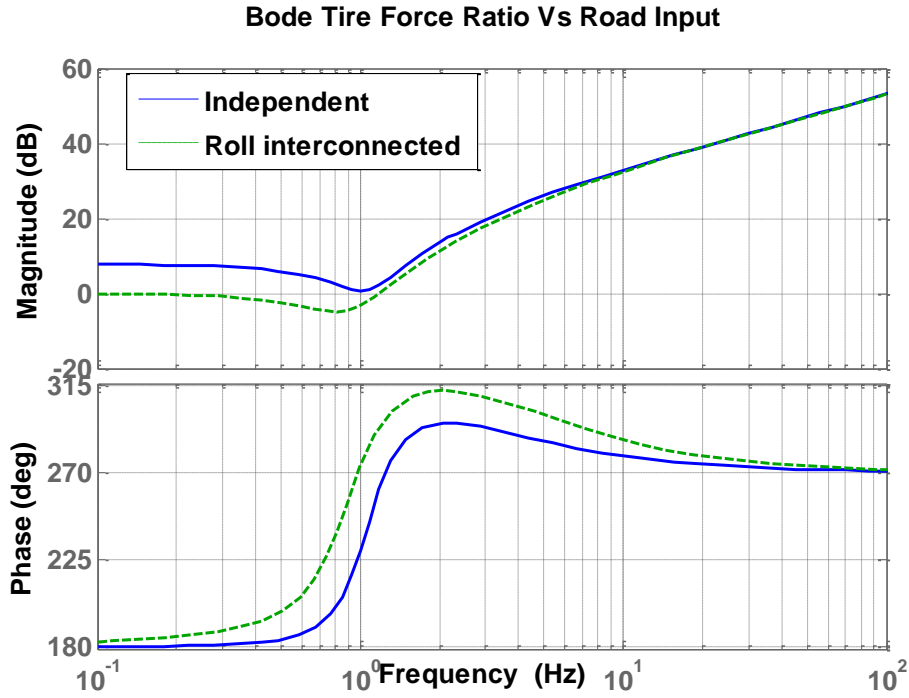


Figure 28- Right and left tires force ratio

As Figure 28 demonstrates, the roll interconnected system does not provide any benefit in high frequencies, but works better than independent system in low frequencies (less than 1 Hertz) in terms of more even load distribution. As it can be seen in bode plots and analytical transfer functions, roll interconnection improves the load distribution in low speeds (low frequencies). In high speeds, the behavior of both systems is the same.

The roll stiffness is defined based on the angular roll displacement of sprung body ($\Delta\phi$) against the applied torque on the body by:

$$\tau - (K_r L_w \Delta\phi + K_t L_w \Delta\phi) L_w - K_t \Delta\phi = 0$$

$$K_{Tor} = \frac{\tau}{\Delta\phi} = 2KL_w^2 + K_t \quad (4.40)$$

where K_t is the torsional stiffness of the axle or anti roll bar.

For a simplified roll interconnected model, torsional stiffness is:

$$\tau - \left(2K \left(\frac{L_w \Delta\phi - L_w \Delta\phi}{2} \right) \right) L_w - K_t \Delta\phi = 0 \quad (4.41)$$

$$K_{Tor_Roll_Int} = \frac{\tau}{\Delta\phi} = K_t$$

The roll interconnected air suspensions exert the same force in the same direction that cancel out each other's moment about the center of mass. As such, the roll interconnected system does not have any returning force or moment to balance the body at the nominal position after applying external force or moment, except the torque comes from the torsional stiffness of axle or anti roll bar. With a complete roll interconnected system, roll response of the sprung body will be slow.

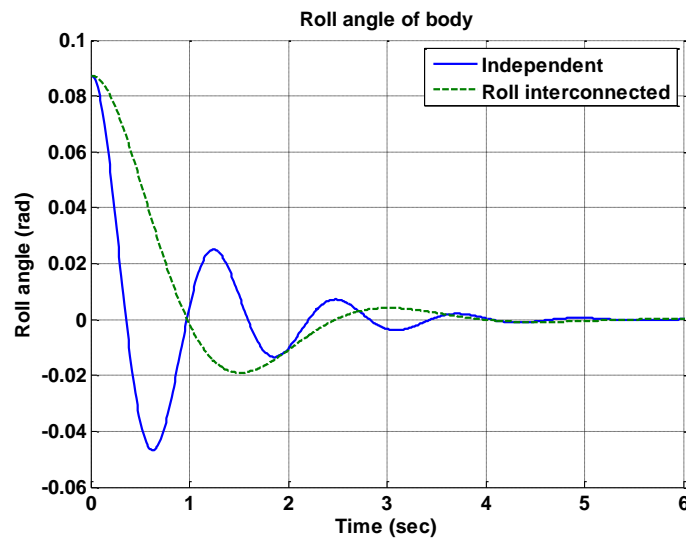


Figure 29- Roll angle of sprung body

Figure 29 shows the time response of the sprung body when 5 degrees (0.087 rad) initial roll angle is applied to the body. The roll interconnected system returns slowly.

Chapter 5 Conclusion and Future Work

Mathematical modeling exhibits an applicable design for air suspension system with ride height and stiffness tuning. An optimum suspension design can be found based on any vehicle specifications and the air suspension model. In the development of the model and design procedure, several design constraints were considered. The minimum accumulators' volume equations were derived based on the minimum and maximum desired natural frequencies with considering the minimum and maximum working pressures. Moreover, air spring dimensions were found according to the minimum accumulators' volume and geometrical constraints. After analyzing the new air suspension design, the equations for setting the air chamber equilibrium pressures were derived to keep vehicle at any desired ride height with extra load.

Future work includes detailed manufacturing design and fabrication of the air suspension system with ride height and stiffness tuning. Also, prototyping and testing will provide valuable information to validate the theoretical modeling and further revision.

Results from the interconnection of air suspensions showed that interconnection is more useful in low speeds and off-road conditions. The pitch interconnection is the best configuration in terms of load distribution between the tandem tires. While all the interconnected configurations worked well in general road simulations, they all suffered from lower roll interconnected system. It was shown that the roll, cross, and all interconnection configurations would deteriorate roll stiffness that in turn deteriorate vehicle handling at higher speeds. Since on off-road, vehicle's speed is necessarily low, interconnection will not have adverse effects on vehicle handling. However, the main configurations could be combined depending on the vehicle application or driving conditions.

Bibliography

- [1] Uys, P. E., Pieter Schalk Els, and M. Thoresson. "Suspension settings for optimal ride comfort of off-road vehicles travelling on roads with different roughness and speeds." *Journal of Terramechanics* 44.2 (2007): 163-175.
- [2] International Organization for Standardization. *Mechanical vibration and shock-Evaluation of human exposure to whole-body vibration-Part 1: General requirements*. The Organization, 1997.
- [3] Paddan, G. S., and M. J. Griffin. "Evaluation of whole-body vibration in vehicles." *Journal of Sound and Vibration* 253.1 (2002): 195-213.
- [4] Giacomini, J., and T. M. Hacaambwa. "Performance of ISO2631 and BS6841 Comfort Criteria for Evaluating Automobile Road Vibrations." Department of Mechanical Engineering. The University of Sheffield.
- [5] Irvine, Tom. "Power spectral density Units:[G²/Hz]." (2000).
- [6] Huang, Chiou-Jye, Jung-Shan Lin, and Chung-Cheng Chen. "Road-adaptive algorithm design of half-car active suspension system." *Expert Systems with Applications* 37.6 (2010): 4392-4402.
- [7] Gillespie, Thomas D. *Heavy truck ride*. No. 850001. SAE Technical Paper, 1985.
- [8] Zargar, Bahram. *Model development, validation and nonlinear control of pneumatic suspensions*. University of Ottawa, 2007.
- [9] Gobbi, M., and G. Mastinu. "Analytical description and optimization of the dynamic behaviour of passively suspended road vehicles." *Journal of sound and vibration* 245.3 (2001): 457-481.
- [10] Swevers, Jan, et al. "A model-free control structure for the on-line tuning of the semi-active suspension of a passenger car." *Mechanical Systems and Signal Processing* 21.3 (2007): 1422-1436.

- [11] Sharp, R. S., and S. A. Hassan. "An evaluation of passive automotive suspension systems with variable stiffness and damping parameters." *Vehicle System Dynamics* 15.6 (1986): 335-350.
- [12] Hong, S. R., et al. "Non-dimensional analysis and design of a magnetorheological damper." *Journal of Sound and Vibration* 288.4 (2005): 847-863.
- [13] Parlak, Zekeriya, Tahsin Engin, and İsmail Çallı. "Optimal design of MR damper via finite element analyses of fluid dynamic and magnetic field." *Mechatronics* 22.6 (2012): 890-903.
- [14] Hundal, M. S. "Impact absorber with two-stage, variable area orifice hydraulic damper." *Journal of Sound and Vibration* 50.2 (1977): 195-202.
- [15] Gillespie, Thomas D. "Fundamentals of Vehicle Dynamics. Warrendale, PA: Society of Automotive Engineers." (1992)
- [16] Korand Group. "Detail Design of Two Passenger Electric Car" Tehran University, (2008): 88-102.
- [17] Rajamani, Rajesh. *Vehicle dynamics and control*. Springer, 2011.
- [18] Williams, R. A. "Automotive active suspensions Part 2: Practical considerations." *Proceedings of the Institution of Mechanical Engineers, Part D: Journal of Automobile Engineering* 211.6 (1997): 415-426.
- [19] Matschinsky, Wolfgang. "Road vehicle suspensions." (2000).
- [20] Chang, F., and Z. H. Lu. "Dynamic model of an air spring and integration into a vehicle dynamics model." *Proceedings of the Institution of Mechanical Engineers, Part D: Journal of Automobile Engineering* 222.10 (2008): 1813-1825.
- [21] Deo, Hrishikesh V. *Axiomatic design of customizable automotive suspension systems*. Diss. Massachusetts Institute of Technology, 2006.
- [22] Toyofuku, Katsuya, et al. "Study on dynamic characteristic analysis of air spring with auxiliary chamber." *JSAE review* 20.3 (1999): 349-355.
- [23] Giliomee, C. L., and P. S. Els. "Semi-active hydropneumatic spring and damper system." *Journal of Terramechanics* 35.2 (1998): 109-117.

- [24] Ramsbottom, M., and D. A. Crolla. "Development and analysis of a prototype controllable suspension." *Training 2014* (1997): 01-15.
- [25] Porumamilla, H., A. G. Kelkar, and J. M. Vogel. "Modeling and verification of an innovative active pneumatic vibration isolation system." *Journal of Dynamic Systems, Measurement, and Control* 130.3 (2008): 031001.
- [26] Yin, Zhihong, et al. "A new pneumatic suspension system with independent stiffness and ride height tuning capabilities." *Vehicle system dynamics* 50.12 (2012): 1735-1746.
- [27] Hawley, Jesse B. "B HAWLEY." U.S. Patent No. 1,984,019. 11 Dec. 1934.
- [28] Pevsner, J. M. "Equalizing types of suspension." *Automobile Engineer* 1 (1957): 10-16.
- [29] Tanahashi, Haruhiko, et al. "Toyota electronic modulated air suspension for the 1986 Soarer." *Internal Combustion Engines* 1997 (1987): 10-02.
- [30] Iijima, Tetsuya, et al. "Development of a hydraulic active suspension." *SAE TRANSACTIONS* 102 (1993): 2142-2142.
- [31] Bhave, S. Y. "Effect of connecting the front and rear air suspensions of a vehicle on the transmissibility of road undulation inputs." *Vehicle System Dynamics* 21.1 (1992): 225-245.
- [32] Ortiz, M. "Principles of interconnected suspensions." *RaceCar Engineering* 7.7-8 (1997).
- [33] Cao, D., S. Rakheja, and C. Y. Su. "Pitch plane analysis of a twin-gas-chamber strut suspension." *Proceedings of the Institution of Mechanical Engineers, Part D: Journal of Automobile Engineering* 222.8 (2008): 1313-1335.
- [34] Cao, Dongpu, Subhash Rakheja, and Chun-Yi Su. "Property Analysis of an X-coupled suspension for sport utility vehicles." *SAE International Journal of Passenger Cars-Mechanical Systems* 1.1 (2009): 853-862.
- [35] Cao, Dongpu, Subhash Rakheja, and Chun-Yi Su. "Pitch attitude control and braking performance analysis of heavy vehicle with interconnected suspensions." *Training 2013* (2007): 04-09.
- [36] Cao, Dongpu, Subhash Rakheja, and Chun-Yi Su. "Comparison of roll properties of hydraulically and pneumatically interconnected suspensions for heavy vehicles." (2005).

- [37] Ding, Fei, et al. "Design of Hydraulically Interconnected Suspension Systems for Tri-axle Straight Trucks with Rear Tandem Axle Bogie Suspensions." *SAE International Journal of Commercial Vehicles* 6.1 (2013): 200-208.
- [38] Wong, Adrian. "Novel Semi-Active Suspension with Tunable Stiffness and Damping." University of Waterloo (2012)

Appendix 1

This appendix is about dynamic equations for four bar linkage used in the air suspension system with two air chambers. The goal is calculating the effective location of axle attached to the trailing arm by the four bar linkage. Figure 30 shows the essential geometry details of dual chamber air suspension system. Blue circle shows the axle and the pivot point has picked as the coordinate origin.

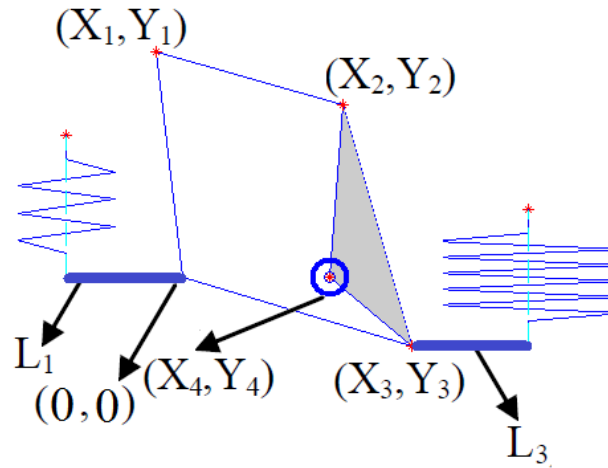


Figure 30- Dual chamber air suspension schematic

Writing the dynamic equilibrium equation concludes to:

$$\begin{aligned} \theta &= \tan^{-1} \left(\frac{Y_1 - Y_2}{X_1 - X_2} \right) \\ p &= X_3 - X_2 \\ q &= X_2 - X_4 \\ r &= Y_2 - Y_3 \\ L_{ax} &= X_3 \left(\frac{r \cos \theta + q \sin \theta}{r \cos \theta - p \sin \theta} \right) \end{aligned} \quad (4.42)$$

Finally, the equivalent stiffness at the axle point is:

$$\begin{aligned} L_2 &= X_3 + L_3 & \frac{L_1}{L_{ax}} &= a & \frac{L_2}{L_{ax}} &= b \\ K_{eq} &= a^2 K_1 + b^2 K_2 \end{aligned} \quad (4.43)$$

Appendix 2

```
clear all
clc
close all
%%%%%%%%%%%%%%%%%%%%%%%%%%%%%%%%%%%%%%%%%%%%%%%%%%%%%%%%%%%%%%%%%%%%%%%% Parameters %%%%%%%%%
load('Road_Profile_4.mat','x','z');
L=990; % m
Vtest=10; % m/s
Tfinal=L/Vtest;
Tstep=0.1/Vtest;
ttest=0:Tstep:Tfinal-Tstep;
%%%%%%%%%%%%%%%%%%%%%%%%%%%%%%%%%%%%%%%%%%%%%%%%%%%%%%%%%%%%%%%%%%%%%%%%
iff=0; jff=0;
ir=1; jr=1;
il=1; jl=1; %%%%%%%%%
im=1; jm=1; %% Interconnection %%
ib=1; jb=1; %%%%%%%%%
icr=1; jcr=1;
icl=1; jcl=1;
%%%%%%%%%%%%%%%%%%%%%%%%%%%%%%%%%%%%%%%%%%%%%%%%%%%%%%%%%%%%%%%%%%%%%%%%
Lf=5; %198*0.0254
Lm=0.5; %22*0.0254
Lb=2; %76*0.0254
Lw=0.9; %35.6*0.0254;
Ltot=Lf+Lb;
Ms=26000;
Mu=200;
Isx=50000;
Isy=150000;
Ksf=333000/2;
Ksr=233000;
K_sf=0;
K_sr=100000;
Ktf=0;
Ktr=800000;
Csf=25000/2;
Csr=25000;
Ku=5000000;
Cu=0;
Kuf=Ku/2;
Kur=Ku;
Cuf=Cu/2;
Cur=Cu;
%%%%%%%%%%%%%%%%%%%%%%%%%%%%%%%%%%%%%%%%%%%%%%%%%%%%%%%%%%%%%%%%%%%%%%%%
a11= -(2*Csf+4*Csr)/Ms;
a12= -(2*Lf*Csf- 2*(Lm+Lb)*Csr)/Ms;
a21= -(2*Lf*Csf- 2*(Lm+Lb)*Csr)/Isy;
a22= -(2*Lf^2*Csf+ 2*(Lm^2+Lb^2)*Csr)/Isy;
a33= -(Lw^2*(2*Csf+4*Csr))/Isx;

a110= -(2*Ksf+4*Ksr)/Ms;
a111= -(2*Lf*Ksf- 2*(Lm+Lb)*Ksr)/Ms;
a210= -(2*Lf*Ksf- 2*(Lm+Lb)*Ksr)/Isy;
```

```

a211= -(2*Lf^2*Ksf+ (2*(Lm^2+Lb^2)-sign(ir+il+icr+icl)*(Lm-Lb)^2)*Ksr)/Isy;
a312= -(Lw^2*(2*Ksf*(1-iff)+4*Ksr*(1-
sign(im+ib+icr+icl))+(Ktf+2*Ktr)/Lw^2))/Isx;

```

```

a14=Csf/Ms;          a41=Csf/Mu;
a15=Csf/Ms;          a51=Csf/Mu;
a16=Csr/Ms;          a61=Csr/Mu;
a17=Csr/Ms;          a71=Csr/Mu;
a18=Csr/Ms;          a81=Csr/Mu;
a19=Csr/Ms;          a91=Csr/Mu;
a24=(Lf*Csf)/Isy;   a42=(Lf*Csf)/Mu;
a25=(Lf*Csf)/Isy;   a52=(Lf*Csf)/Mu;
a26=(-Lm*Csr)/Isy;  a62=(-Lm*Csr)/Mu;
a27=(-Lm*Csf)/Isy;  a72=(-Lm*Csr)/Mu;
a28=(-Lb*Csr)/Isy;  a82=(-Lb*Csr)/Mu;
a29=(-Lb*Csr)/Isy;  a92=(-Lb*Csr)/Mu;
a34=(Lw*Csf)/Isx;   a43=(Lw*Csf)/Mu;
a35=(-Lw*Csf)/Isx;  a53=(-Lw*Csf)/Mu;
a36=(Lw*Csr)/Isx;   a63=(Lw*Csr)/Mu;
a37=(-Lw*Csr)/Isx;  a73=(-Lw*Csr)/Mu;
a38=(Lw*Csr)/Isx;   a83=(Lw*Csr)/Mu;
a39=(-Lw*Csr)/Isx;  a93=(-Lw*Csr)/Mu;

```

```

a44=- (Csf+Cuf)/Mu;
a55=- (Csf+Cuf)/Mu;
a66=- (Csr+Cur)/Mu;
a77=- (Csr+Cur)/Mu;
a88=- (Csr+Cur)/Mu;
a99=- (Csr+Cur)/Mu;

```

```

i1=(Lm*(1+im)+Lb*(ir+icr))/(1+im+ir+icr);
i2=(Lm*(1+im)+Lb*(il+icl))/(1+im+il+icl);
i3=(Lb*(1+ib)+Lm*(ir+icl))/(1+ib+ir+icl);
i4=(Lb*(1+ib)+Lm*(il+icr))/(1+ib+il+icr);
i5=(Lw*(1-im+ir-icr))/(1+im+ir+icr);
i6=(Lw*(1-im+il-icl))/(1+im+il+icl);
i7=(Lw*(1-ib+ir-icl))/(1+ib+ir+icl);
i8=(Lw*(1-ib+il-icr))/(1+ib+il+icr);
i9=(Lf*(1+iff))/(1+iff);
i10=(Lw*(1-iff))/(1+iff);
i11=(1+im+ir+icr);
i12=(1+im+il+icl);
i13=(1+ib+ir+icl);
i14=(1+ib+il+icr);

```

```

a113=Ksf/Ms;          a410=Ksf/Mu;
a114=Ksf/Ms;          a510=Ksf/Mu;
a115=Ksr/Ms;          a610=Ksr/Mu;
a116=Ksr/Ms;          a710=Ksr/Mu;
a117=Ksr/Ms;          a810=Ksr/Mu;
a118=Ksr/Ms;          a910=Ksr/Mu;
a213=(i9*Ksf)/Isy;   a411=(i9*Ksf)/Mu;
a214=(i9*Ksf)/Isy;   a511=(i9*Ksf)/Mu;
a215=(-i1*Ksr)/Isy;  a611=(-i1*Ksr)/Mu;

```

```

a216=(-i2*Ksr)/Isy;
a217=(-i3*Ksr)/Isy;
a218=(-i4*Ksr)/Isy;
a313=(i10*Ksf+(Ktf/(2*Lw)))/Isx;
a314=(-i10*Ksf-(Ktf/(2*Lw)))/Isx;
a315=(i5*Ksr+(Ktr/(2*Lw)))/Isx;
a316=(-i6*Ksr-(Ktr/(2*Lw)))/Isx;
a317=(i7*Ksr+(Ktr/(2*Lw)))/Isx;
a318=(-i8*Ksr-(Ktr/(2*Lw)))/Isx;

b11=Cuf/Mu;
b22=Cuf/Mu;
b33=Cur/Mu;
b44=Cur/Mu;
b55=Cur/Mu;
b66=Cur/Mu;

e110= -(2*K_sf+4*K_sr)/Ms;
e111= -(2*Lf*K_sf- 2*(Lm+Lb)*K_sr)/Ms;
e210= -(2*Lf*K_sf- 2*(Lm+Lb)*K_sr)/Isy;
e211= -(2*Lf^2*K_sf+ (2*(Lm^2+Lb^2)-sign(jr+jl+jcr+jcl))*(Lm-Lb)^2)*K_sr)/Isy;
e312= -(Lw^2*(2*K_sf*(1-jff)+4*K_sr*(1-sign(jm+jb+jcr+jcl))))/Isx;

j1=(Lm*(1+jm)+Lb*(jr+jcr))/(1+jm+jr+jcr);
j2=(Lm*(1+jm)+Lb*(jl+jcl))/(1+jm+jl+jcl);
j3=(Lb*(1+jb)+Lm*(jr+jcl))/(1+jb+jr+jcl);
j4=(Lb*(1+jb)+Lm*(jl+jcr))/(1+jb+jl+jcr);
j5=(Lw*(1-jm+jr-jcr))/(1+jm+jr+jcr);
j6=(Lw*(1-jm+jl-jcl))/(1+jm+jl+jcl);
j7=(Lw*(1-jb+jr-jcl))/(1+jb+jr+jcl);
j8=(Lw*(1-jb+jl-jcr))/(1+jb+jl+jcr);
j9=(Lf*(1+jff))/(1+jff);
j10=(Lw*(1-jff))/(1+jff);
j11=(1+jm+jr+jcr);
j12=(1+jm+jl+jcl);
j13=(1+jb+jr+jcl);
j14=(1+jb+jl+jcr);

e113=K_sf/Ms;
e114=K_sf/Ms;
e115=K_sr/Ms;
e116=K_sr/Ms;
e117=K_sr/Ms;
e118=K_sr/Ms;
e213=(j9*K_sf)/Isy;
e214=(j9*K_sf)/Isy;
e215=(-j1*K_sr)/Isy;
e216=(-j2*K_sr)/Isy;
e217=(-j3*K_sr)/Isy;
e218=(-j4*K_sr)/Isy;
e313=(j10*K_sf)/Isx;
e314=(-j10*K_sf)/Isx;
e315=(j5*K_sr)/Isx;
e316=(-j6*K_sr)/Isx;
e317=(j7*K_sr)/Isx;

a711=(-i2*Ksr)/Mu;
a811=(-i3*Ksr)/Mu;
a911=(-i4*Ksr)/Mu;
a412=(i10*Ksf+(Ktf/(2*Lw)))/Mu;
a512=(-i10*Ksf-(Ktf/(2*Lw)))/Mu;
a612=(i5*Ksr+(Ktr/(2*Lw)))/Mu;
a712=(-i6*Ksr-(Ktr/(2*Lw)))/Mu;
a812=(i7*Ksr+(Ktr/(2*Lw)))/Mu;
a912=(-i8*Ksr-(Ktr/(2*Lw)))/Mu;

b17=Kuf/Mu;
b28=Kuf/Mu;
b39=Kur/Mu;
b410=Kur/Mu;
b511=Kur/Mu;
b612=Kur/Mu;

e410=K_sf/Mu;
e510=K_sf/Mu;
e610=K_sr/Mu;
e710=K_sr/Mu;
e810=K_sr/Mu;
e910=K_sr/Mu;
e411=(j9*K_sf)/Mu;
e511=(j9*K_sf)/Mu;
e611=(-j1*K_sr)/Mu;
e711=(-j2*K_sr)/Mu;
e811=(-j3*K_sr)/Mu;
e911=(-j4*K_sr)/Mu;
e412=(j10*K_sf)/Mu;
e512=(-j10*K_sf)/Mu;
e612=(j5*K_sr)/Mu;
e712=(-j6*K_sr)/Mu;
e812=(j7*K_sr)/Mu;

```

```

e318=(-j8*K_sr)/Isx;
e912=(-j8*K_sr)/Mu;

a413=-(Ksf/(1+iff) + Kuf)/Mu;
a514=-(Ksf/(1+iff) + Kuf)/Mu;
a414=-(Ksf*iff)/(Mu*(1+iff));
a513=-(Ksf*iff)/(Mu*(1+iff));
a615=-(Ksr/il1 + Kur)/Mu;
a716=-(Ksr/il2 + Kur)/Mu;
a817=-(Ksr/il3 + Kur)/Mu;
a918=-(Ksr/il4 + Kur)/Mu;
a715=-(Ksr*im)/(Mu*i11);
a815=-(Ksr*ir)/(Mu*i11);
a915=-(Ksr*icr)/(Mu*i11);
a616=-(Ksr*im)/(Mu*i12);
a816=-(Ksr*icl)/(Mu*i12);
a916=-(Ksr*il)/(Mu*i12);
a617=-(Ksr*ir)/(Mu*i13);
a717=-(Ksr*icl)/(Mu*i13);
a917=-(Ksr*ib)/(Mu*i13);
a618=-(Ksr*icr)/(Mu*i14);
a718=-(Ksr*il)/(Mu*i14);
a818=-(Ksr*ib)/(Mu*i14);

e413=-(K_sf/(1+jff))/Mu;
e514=-(K_sf/(1+jff))/Mu;
e414=-(K_sf*jff)/(Mu*(1+jff));
e513=-(K_sf*jff)/(Mu*(1+jff));
e615=-(K_sr/j11)/Mu;
e716=-(K_sr/j12)/Mu;
e817=-(K_sr/j13)/Mu;
e918=-(K_sr/j14)/Mu;
e715=-(K_sr*jm)/(Mu*j11);
e815=-(K_sr*jr)/(Mu*j11);
e915=-(K_sr*jcr)/(Mu*j11);
e616=-(K_sr*jm)/(Mu*j12);
e816=-(K_sr*jcl)/(Mu*j12);
e916=-(K_sr*j1)/(Mu*j12);
e617=-(K_sr*jr)/(Mu*j13);
e717=-(K_sr*jcl)/(Mu*j13);
e917=-(K_sr*j1)/(Mu*j13);
e618=-(K_sr*jcr)/(Mu*j14);
e718=-(K_sr*j1)/(Mu*j14);
e818=-(K_sr*j1)/(Mu*j14);

```

```

CMAT=[a11 a12 0 a14 a15 a16 a17 a18 a19;
      a21 a22 0 a24 a25 a26 a27 a28 a29;
      0 0 a33 a34 a35 a36 a37 a38 a39 ;
      a41 a42 a43 a44 0 0 0 0 0 ;
      a51 a52 a53 0 a55 0 0 0 0 ;
      a61 a62 a63 0 0 a66 0 0 0 ;
      a71 a72 a73 0 0 0 a77 0 0 ;
      a81 a82 a83 0 0 0 0 a88 0 ;
      a91 a92 a93 0 0 0 0 0 a99];

```

```

KMAT=[a110 a111 0 a113 a114 a115 a116 a117 a118;
      a210 a211 0 a213 a214 a215 a216 a217 a218;
      0 0 a312 a313 a314 a315 a316 a317 a318;
      a410 a411 a412 a413 a414 0 0 0 0 ;
      a510 a511 a512 a513 a514 0 0 0 0 ;
      a610 a611 a612 0 0 a615 a616 a617 a618;
      a710 a711 a712 0 0 a715 a716 a717 a718;
      a810 a811 a812 0 0 a815 a816 a817 a818;
      a910 a911 a912 0 0 a915 a916 a917 a918];

```

```

K_MAT=[e110 e111 0 e113 e114 e115 e116 e117 e118;
      e210 e211 0 e213 e214 e215 e216 e217 e218;
      0 0 e312 e313 e314 e315 e316 e317 e318;
      e410 e411 e412 e413 e414 0 0 0 0 ;
      e510 e511 e512 e513 e514 0 0 0 0 ;
      e610 e611 e612 0 0 e615 e616 e617 e618;
      e710 e711 e712 0 0 e715 e716 e717 e718;
      e810 e811 e812 0 0 e815 e816 e817 e818;
      e910 e911 e912 0 0 e915 e916 e917 e918];

```

```

A=[CMAT KMAT+K_MAT; eye(9,9) zeros(9,9)];

```

```

B=[ 0 0 0 0 0 0 0 0 0 0 0 0 ;
    0 0 0 0 0 0 0 0 0 0 0 0 ;
    0 0 0 0 0 0 0 0 0 0 0 0 ;
    b11 0 0 0 0 0 b17 0 0 0 0 0 ;
    0 b22 0 0 0 0 0 b28 0 0 0 0 ;
    0 0 b33 0 0 0 0 0 b39 0 0 0 ;
    0 0 0 b44 0 0 0 0 0 b410 0 0 ;
    0 0 0 0 b55 0 0 0 0 0 b511 0 ;
    0 0 0 0 0 b66 0 0 0 0 0 b612;
    0 0 0 0 0 0 0 0 0 0 0 0 ;
    0 0 0 0 0 0 0 0 0 0 0 0 ;
    0 0 0 0 0 0 0 0 0 0 0 0 ;
    0 0 0 0 0 0 0 0 0 0 0 0 ;
    0 0 0 0 0 0 0 0 0 0 0 0 ;
    0 0 0 0 0 0 0 0 0 0 0 0 ;
    0 0 0 0 0 0 0 0 0 0 0 0 ;
    0 0 0 0 0 0 0 0 0 0 0 0 ];

C=[ 0 0 0 0 0 0 0 0 0 0 0 0 -Kuf 0 0 0 0 0 ;
    0 0 0 0 0 0 0 0 0 0 0 0 0 -Kuf 0 0 0 0 ;
    0 0 0 0 0 0 0 0 0 0 0 0 0 0 -Kur 0 0 0 ;
    0 0 0 0 0 0 0 0 0 0 0 0 0 0 0 -Kur 0 0 ;
    0 0 0 0 0 0 0 0 0 0 0 0 0 0 0 0 -Kur 0 ;
    0 0 0 0 0 0 0 0 0 0 0 0 0 0 0 0 0 Kur];

D=[ 0 0 0 0 0 0 Kuf 0 0 0 0 0 ;
    0 0 0 0 0 0 0 Kuf 0 0 0 0 ;
    0 0 0 0 0 0 0 0 Kur 0 0 0 ;
    0 0 0 0 0 0 0 0 0 Kur 0 0 ;
    0 0 0 0 0 0 0 0 0 0 Kur 0 ;
    0 0 0 0 0 0 0 0 0 0 0 Kur ];

%*****
CC=[ 0 0 0 0 0 0 0 0 0 1 Lf Lw 0 0 0 0 0 0 ;
    0 0 0 0 0 0 0 0 0 0 1 Lf -Lw 0 0 0 0 0 0 ;
    0 0 0 0 0 0 0 0 0 0 1 -Lm Lw 0 0 0 0 0 0 ;
    0 0 0 0 0 0 0 0 0 0 1 -Lm -Lw 0 0 0 0 0 0 ;
    0 0 0 0 0 0 0 0 0 0 1 -Lb Lw 0 0 0 0 0 0 ;
    0 0 0 0 0 0 0 0 0 0 1 -Lb -Lw 0 0 0 0 0 0 ];

DD=zeros(6,12);
%*****
CS=eye(18);
DS=zeros(18,12);
%*****
sys=ss(A,B,C,D);
sys1=ss(A,B,CC,DD);
sys2=ss(A,B,CS,DS);

Zg=z(10*(Ltot/2)+1:10*(L+(Ltot/2)));
zz=fliplr(z);
Zgfr=z(10*Ltot+1:10*(L+Ltot));
Zgfl=zz(10*Ltot+1:10*(L+Ltot));

```

```

Zgmr=z(10*(Lb-Lm)+1:10*(L+(Lb-Lm)));
Zgml=zz(10*(Lb-Lm)+1:10*(L+(Lb-Lm)));
Zgbr=z(1:10*L);
Zgbl=zz(1:10*L);

Zdgfr=diff(Zgfr)/Tstep;
Zdgfr(size(Zdgfr,2)+1)=2*Zdgfr(size(Zdgfr,2))-Zdgfr(size(Zdgfr,2)-1);
Zdgmr=diff(Zgmr)/Tstep;
Zdgmr(size(Zdgmr,2)+1)=2*Zdgmr(size(Zdgmr,2))-Zdgmr(size(Zdgmr,2)-1);
Zdgbr=diff(Zgbr)/Tstep;
Zdgbr(size(Zdgbr,2)+1)=2*Zdgbr(size(Zdgbr,2))-Zdgbr(size(Zdgbr,2)-1);
Zdgfl=diff(Zgfl)/Tstep;
Zdgfl(size(Zdgfl,2)+1)=2*Zdgfl(size(Zdgfl,2))-Zdgfl(size(Zdgfl,2)-1);
Zdgml=diff(Zgml)/Tstep;
Zdgml(size(Zdgml,2)+1)=2*Zdgml(size(Zdgml,2))-Zdgml(size(Zdgml,2)-1);
Zdgb1=diff(Zgbl)/Tstep;
Zdgb1(size(Zdgb1,2)+1)=2*Zdgb1(size(Zdgb1,2))-Zdgb1(size(Zdgb1,2)-1);

U=[Zdgfr; Zdgfl; Zdgmr; Zdgml; Zdgbr; Zdgb1; Zgfr; Zgfl; Zgmr; Zgml; Zgbr;
Zgbl; ];

[Y,t]=lsim(sys,U,ttest);
[YS,t]=lsim(sys2,U,ttest);

RMS_MAX_Force=zeros(6,2);
for j=1:1:6
    RMS_MAX_Force(j,1) = sqrt(mean(Y(:,j).^2));
    RMS_MAX_Force(j,2) = max(Y(100:10*L,j));
end
RMS_MAX_Force

RMS_MAX_Kin=zeros(3,2);
for j=10:1:12
    RMS_MAX_Kin(j-9,1) = sqrt(mean(YS(:,j).^2)) * 180/pi;
    RMS_MAX_Kin(j-9,2) = max(YS(100:10*L,j)) * 180/pi;
end
RMS_MAX_Kin

AA=eig(A);
NF_DR=zeros(9,2);
for j=1:2:17
    NF(j/2 + 0.5 , 1)= sqrt((real(AA(j)))^2+(imag(AA(j)))^2) / (2*pi);
    NF(j/2 + 0.5 , 2)= -real(AA(j)) / sqrt((real(AA(j)))^2+(imag(AA(j)))^2);
end
NF;

i=3; %TFs respect to middle tire
[b,a]=ss2tf(A,B,C,D,i+6);

Gm_m=tf(b(3,:),a);
Gb_m=tf(b(5,:),a);
Gml_m=tf(b(4,:),a);
Gbl_m=tf(b(6,:),a);

```

```

GRb_m=tf(b(i,:),b(5,:));
GRml_m=tf(b(i,:),b(4,:));
GRbl_m=tf(b(i,:),b(6,:));

i=5; %TFs respect to back tire
[b,a]=ss2tf(A,B,C,D,i+6);

Gm_b=tf(b(3,:),a);
Gb_b=tf(b(5,:),a);
Gml_b=tf(b(4,:),a);
Gbl_b=tf(b(6,:),a);

GRm_b=tf(b(i,:),b(3,:));
GRml_b=tf(b(i,:),b(4,:));
GRbl_b=tf(b(i,:),b(6,:));

i = 3; % or 5
[b,a]=ss2tf(A,B,CC,DD,i+6);
aa1=a;
bb1=b(1,:);
GG1=tf(bb1,aa1);

aa2=a;
bb2=b(2,:);
GG2=tf(bb2,aa2);

aa3=a;
bb3=b(3,:);
GG3=tf(bb3,aa3);

aa4=a;
bb4=b(4,:);
GG4=tf(bb4,aa4);

aa5=a;
bb5=b(5,:);
GG5=tf(bb5,aa5);

aa6=a;
bb6=b(6,:);
GG6=tf(bb6,aa6);

[b,a]=ss2tf(A,B,CS,DS,i+6);
aa1=a;
bh1=b(10,:);
bp1=b(11,:);
br1=b(12,:);
GSbounce=tf(bh1,aa1);
GSpitch=tf(bp1,aa1);
GSroll=tf(br1,aa1);

```